Investigation of Single Fiber Composite residual strength pre and post fragmentation: Using Progressive Damage Analysis and HFGMC framework

Mr. Pankaj Pandya

A Thesis Submitted to
Indian Institute of Technology Hyderabad
In Partial Fulfillment of the Requirements for
The Degree of Master of Technology

भारतीय प्रौद्योगिकी संस्थान हैदराबाद
Indian Institute of Technology Hyderabad

Department of Mechanical and Aerospace Engineering

July 2017

Declaration

I declare that this written submission represents my ideas in my own words, and where ideas or words of others have been included, I have adequately cited and referenced the original sources. I also declare that I have adhered to all principles of academic honesty and integrity and have not misrepresented or fabricated or falsified any idea/data/fact/source in my submission. I understand that any violation of the above will be a cause for disciplinary action by the Institute and can also evoke penal action from the sources that have thus not been properly cited, or from whom proper permission has not been taken when needed.

Pankaj

(Signature)

PANKAJ PANDYA
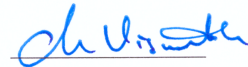
(Mr. Pankaj Pandya)

ME15MTECH11026

(Roll No.)

Approval Sheet

This Thesis entitled Investigation of Single Fiber Composite residual strength pre and post fragmentation: Using Progressive Damage Analysis and HFGMC framework by Mr. Pankaj Pandya is approved for the degree of Master of Technology from IIT Hyderabad

(Dr. Prashant Saxena) Examiner
Dept. of Mechanical & Aerospace Engineering
IITH

(Dr. Viswanath Chinthapenta) Adviser
Dept. of Mechanical & Aerospace Engineering
IITH

(Dr. Seetha N) Chairman
Dept. of Civil Engineering
IITH

Acknowledgements

Dedication

To my friends

Abstract

Single fiber composites (SFC) provides an insight of damage behavior in the fiber reinforced polymer (FRP). Study of stress redistribution after the fiber breakage in the SFC reveals the development of different damage modes that occur in FRPs. Two separate analysis are presented in the current work. The first one being the effective property calculation of multi fiber composite and the second is the analysis of the fiber breakage in the SFC under tensile loading in the direction of the fiber. Analysis of multi fiber composite is carried out using the representative volume element of SFC (SFC-RVE) with periodic boundary conditions. High Fidelity Generalized Method of Cells (HFGMC) has been used for the stress analysis to capture the influence of the length scales in both SFC-RVE and SFC fiber fragmentation test. Progressive damage in the SFC-RVE is detected using the Multi-Continuum Theory (MCT). The choice of MCT to detect damage is purely based on the convenience to obtain the single damage metric in the SFC-RVE analysis. In order to detect the damage of fiber in SFC with fiber fragmentation test, a maximum stress criterion is employed. Further, the use of sudden material property degradation rule is common to both SFC-RVE and SFC fiber fragmentation test. It assists in degrading the property of damaged subcells. Above three steps constitutes the progressive damage analysis (PDA) and it is performed numerically in the FORTRAN language.

The analysis of the SFC-RVE determines the average properties of the multi-fiber composite. In the result of SFC fiber fragmentation test, the evolution of matrix crack, fiber-matrix interface failure, stress redistribution around the fiber failure is discussed. Realizing stress interactions along the fiber-matrix interface provides and insight of load transfer from the matrix to the fiber. The effect of fiber fragment length on the strength of fiber is also presented.

Contents

List of Figures

List of Tables

Chapter 1

Introduction to composite materials and their micro-mechanical analysis

1.1 Composite materials

Composite materials are known for their superior mechanical properties. They have a high strength to weight ratio, fatigue life, high stiffness, and corrosion and wear resistance. Composites are the multiphase structure whose constituents are insoluble in each other. It consists of reinforcing phase and the supporting medium. The primary function of reinforcing phase is to take the stress when the composite is loaded. Supporting medium has the function to transfer the external load to the reinforcing phase. Carbon fiber reinforced polymer (CFRP) is one variant of a composite in which the epoxy matrix transfers the load to the carbon fibers. Other examples of composites include ceramic matrix reinforced with carbon matrix.

Composites are classified in three categories [1]. These are fibrous (Figs. 1.1a and 1.1b), laminated (Fig. 1.1c) and particulate composites (Fig. 1.1d). Single fiber composites (SFC) belong to the unidirectional fibrous class of composites. SFC has been introduced in Section 1.2. Its complete exposition is given in Chapter 4.

Extensive use of composites, having improved properties, has made their analysis essential [2]. The analysis of diversely tailored composites is required to predict its behavior under loading. Multi-scale analysis technique helps in predicting the effective response of composites at a global scale while incorporating original microstructure in the micro level analysis. The micromechanical approach also helps in predicting the local behavior of composites at the micro level [3, 4].

1.1.1 Multi-scale analysis of composites

Analysis of a composite material is performed at a global, meso and micro level [5]. At the micro level, composites are composed of its constituents, namely – fiber/inclusions, matrix and interface. At the meso level, micro level constituents combine to form laminae. Furthermore, laminates combine at a global scale to form composite structures. At a micro level, the analysis is performed with

(a) Continuous fiber

(b) Short fiber

(c) Laminated

(d) Particulate
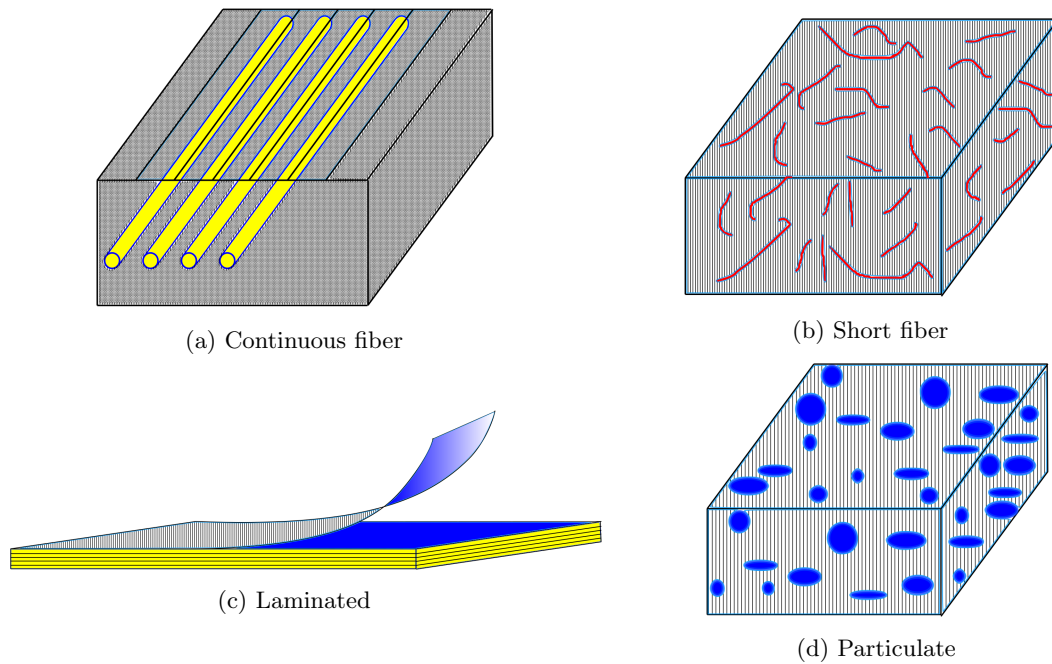
Figure 1.1: Classification of composites

the help of micromechanics which assists in understanding load transfer interactions between the composite's constituent. It provides insight of failure mechanisms in fibers/matrix/interfaces and also gives the information on strength, fatigue life and toughness. However, micromechanics cannot be used at the laminate (meso) level or the structural (global) level due to computational limitations. Consequently, macromechanics is used at the laminate level and its basis is homogenization. Here properties of laminates are averaged between its constituents. Macromechanical techniques are further developed to understand stacks of laminates. Structural analysis is performed at the global scale for understanding overall behavior of composite structures. Localization and homogenization techniques help in linking constituent and structural level.

1.2 Single Fiber composites

Properties of composites significantly depend on the fiber from which it has been manufactured. There are several techniques to calculate the effective properties of fiber in the composite. One way of quantitatively characterizing the fiber in a composite is to conduct tensile testing of single fibers. Experimental work had been performed in this direction by Kumar et al. [6]. Apart from this SFC has been widely used for the quantitative characterization of microscopic damages and interfacial properties in the composites [7]. Fig. 1.2 shows the outline diagram of single fiber embedded in the matrix under tensile loading.

1.2.1 Analysis of Single Fiber Composite

In the present work, micromechanical analysis has been performed to analyze the SFC with fiber breakages in it. To this end, localization has been performed to carry out micromechanical analysis
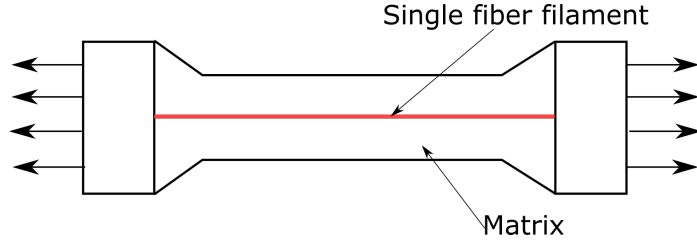
Figure 1.2: Single fiber composite under tensile loading

of fiber breakages in SFC. Further, homogenization is performed to evaluate global response of SFC. Fiber is the main load bearing member in a unidirectional fiber composite under tensile loading. It causes fiber to break into small fragments until damage saturation is achieved. Damage saturation is the state when each fiber has its length less than or equal to the critical length l_c [8, 9]. Critical length l_c is the minimum length of the fiber fragment, such that the stresses in it are just sufficient to fracture the fiber fragment. Eq. (1.1) gives the expression for critical length. Based on the shear lag model critical length has been derived in [10, 11]. The complete formulation of critical length is present in the Section 4.3.1. Here σ_u is the ultimate strength of fiber and τ_m is the shear stress at the fiber-matrix interface.

$$l_c = \frac{\sigma_u d}{2\tau_m} \tag{1.1}$$

Fig. 1.3 helps in understanding stresses present in fiber fragments. Fiber fragments having the
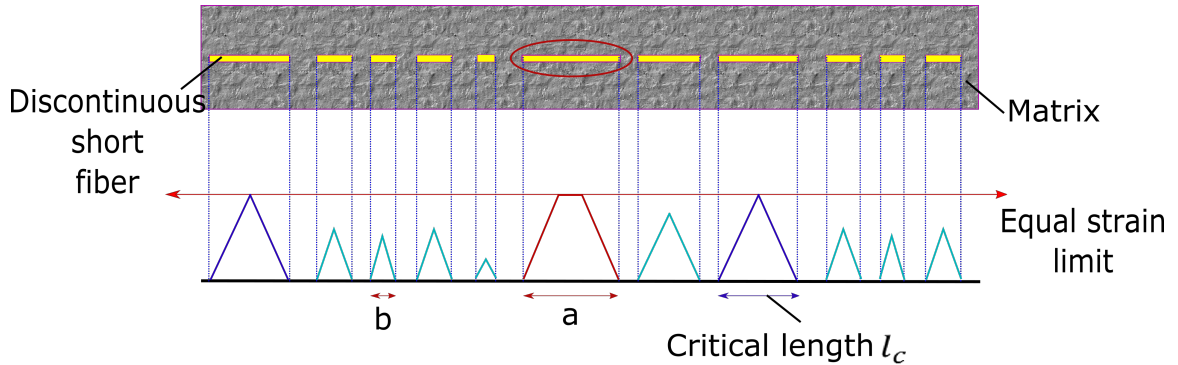
Figure 1.3: Schematic of SFC with fiber fragmentation

length **a** can undergo further fracture as it has a constant stress over its length. On the other hand, fragments of the length b shorter than critical length l_c are having stresses less than the ultimate strength of the fiber. It cannot undergo any further breakage since stresses in it never reach to ultimate fracture stress. The full description of stress development in fiber fragments is available in literature[9].

1.2.2   Types of failure in SFC

Damage in SFC is a complex phenomenon as it consists of multiphase structures. Unidirectional fiber composites are formed with the help of the high strength multiple fibers embedded in the matrix. Fibers are the primary load carrying members while the matrix helps in the load transfer to

the fiber. Thus the composite fails with the multiple fiber failures. Other failure modes undergone by composites are matrix cracking, delamination, fiber-matrix debonding and fiber pull outs.
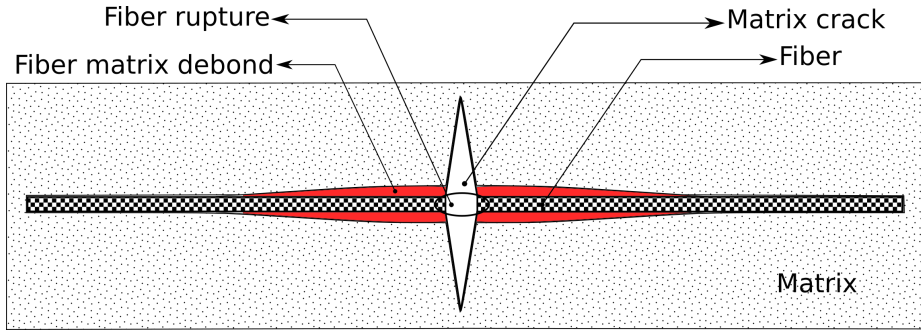
Figure 1.4: Schematic of SFC with fiber fragmentation

Fig. 1.4 show different failure modes that occur in SFC. These are fiber rupture, matrix crack and the fiber matrix debond. The work performed on the analysis of SFC assists in understanding damage modes shown in Fig. 1.4. Besides, stress redistribution and load transfer are also explained based on the analysis of SFC.

1.3 Motivation

Composites find their extensive usage in aeronautics, astronautics, military defense and transportation due to their superior mechanical properties. Analysis of composite materials is essential to ensure its reliability as a structural material. SFC fragmentation test provides important correlation with structural composites. The correlation is present as the SFC display damage mechanisms that are prevalent in multi-fiber composite which is used as structural components [12].

Experimental findings provide essential information on the damage modes that are present in the SFC under tensile loading. Experimental analyses are present in the literature [6, 13]. Experimental procedures lack flexibility as compared to computational methods. In order to address this shortcoming of the experimental procedure, computational methods are developed. The existing progressive damage analysis (PDA) framework allows one to vary material and geometrical parameters such that different composites can be analyzed.

1.4 Objectives

Following are the objectives that have been met in the present work.

- To simulate experimental testing conditions on single fiber composite (SFC)

- To understand the stress redistribution in composites with fiber fragmentation

- To capture stresses responsible for fiber matrix debond

- To analyze the increase in the strength of the fiber with reduction in its length

1.5   Thesis layout

The work presented in the current thesis has been divided into six chapters. Chapter 1 comprises of the introduction about the composites, its constituents, and SFC. Methodologies used in the analysis of SFC has been introduced. Chapter 2 gives the detailed understanding of HFGMC stress analysis method. Effective property calculations has been described at the end of this chapter. Chapter 3 talks about the PDA of SFC. All the three major parts of the PDA are described in this chapter. Derivations pertaining to damage detection module have also been discussed in Chapter 3. Detailed analysis of SFC is presented in the Chapter 4. Besides, the geometrical and material parameter is described towards the end of Chapter 4. Results of the analysis of SFC are discussed in Chapter 5. The work done is concluded in Chapter 6.

Chapter 2

High Fidelity Generalized Method of Cells

2.1 Introduction

High fidelity generalized method of cell (HFGMC) methodology helps in conducting micromechanical stress analysis of inhomogeneous materials. HFGMC is generally used in multi-scale modeling. It predicts average and local strain response based on the constituent properties of a given structure. HFGMC is used for stress analysis since it can adequately capture the local stress transfer mechanism between the fiber and the matrix in composites. Further, it allows the isoparametric subcell generation, thus making it possible to discretize the structure in arbitrary quadrilateral shapes other than squares and rectangles. HFGMC employs the quadratic expression for displacement in the term of local coordinates placed at the centroid of the subcell. Such inclusion of higher order terms helps in conducting transverse shear stress analysis. For understanding the basics of HFGMC concepts, it is necessary to go through the MOC [3] and GMC [14] literature.

HFGMC is the third stage evolution of the technique that works on the subcell discretization of repeating unit cell (RUC). The first two being Method of Cells (MOC) and Generalized Method of Cells (GMC) respectively. The displacement equation for the center of the subcell in the HFGMC is obtained from the MOC. The main difference between HFGMC and MOC is that the former uses up to second order term in its displacement equation while the later uses the first order term. The inclusion of higher order terms in displacement equation helps in capturing the stress field gradients. These stress field gradients are predominantly found at the interface of two different phases of the microstructure [15]. For MOC the displacement equation at the center of a subcell is given by the Eq. (2.1).

$$u_i^{\beta\gamma} = w_i^{\beta\gamma}(\mathbf{x}) + y_2^{\beta}\phi_i^{\beta\gamma} + y_3^{\gamma}\psi_i^{\beta\gamma} \qquad i = 1, 2, 3 \tag{2.1}$$

where $w_i^{\beta\gamma}(\mathbf{x})$ is a displacement corresponding to the center of a subcell, y_2^{β} and y_3^{γ} represents local coordinates within a subcell. Here $(\beta\gamma)$ represents a particular subcell. The coordinates y_2^{β} and y_3^{γ} are related to the displacement $u_i^{\beta\gamma}$ through the $\phi_i^{\beta\gamma}$ and $\psi_i^{\beta\gamma}$ functions respectively. Using MOC approach, one can perform the analysis of composite with elastic fiber and inelastic matrix. It

provides an overall effective constitutive response, calculations of coefficients of thermal expansion, thermal conductivities and specific heat of composite materials. MOC has proved to be an effective tool to calculate average properties of composites but there are several limitations associated with this approach:

- Since the discretization of RUC is limited to four subcells, composites with complex fiber shapes cannot be analyzed.

- It is not possible to analyze the composite with the interface in between matrix and fiber as there are insufficient number of subcells to accommodate the interface material for analysis.

In order to address the limitations of MOC, Generalized Method of Cells (GMC) was derived. In the GMC methodology, RUC can be divided into an arbitrary number of subcells. The generalization of the MOC method extends its capability to analyze composites having the variation in fiber distance and composites having an interface between fiber and matrix. Since in the GMC method, RUC can be divided into an arbitrary number of subcells, it provides a more accurate result for complex structures when compared with the MOC analysis results. GMC method also allows the analysis of structures having three-dimensional periodicity, thus making it possible to analyze composites with discontinuous fibers, foam structures and woven composite structures. Non-linear material models can also be solved with GMC method.

The formulation of GMC method is similar to the MOC method. The first order formulation within the subcell is given below in the Eq. (2.2):

$$u_i^{\alpha\beta\gamma} = w_i^{\alpha\beta\gamma}(\mathbf{x}) + y_1^\alpha \chi_i^{\alpha\beta\gamma} + y_2^\beta \phi_i^{\alpha\beta\gamma} + y_3^\gamma \psi_i^{\alpha\beta\gamma} \qquad i = 1, 2, 3 \qquad (2.2)$$

where $w_i^{\alpha\beta\gamma}(\mathbf{x})$ represents the displacement of the center of subcell. Note that here $(\mathbf{x})$ is a vector and it represents the displacement of the center of subcell with respect to the origin of coordinate system defined globally $(\mathbf{x}_1, \mathbf{x}_2, \mathbf{x}_3)$. The coordinate y_1^α, y_2^β and y_3^γ is corresponding to the local coordinate system within the subcell. $\chi^{\alpha\beta\gamma}$, $\phi^{\alpha\beta\gamma}$ and $\psi^{\alpha\beta\gamma}$ are the weights to characterize the linear displacement within the subcell with respect to the local coordinate system.

GMC method overcomes the limitation of MOC. In GMC, RUC is discretized in an arbitrary fashion to capture the complex microstructure present in a composite. However, the main drawback of GMC is the lack in capturing shear coupling. Aboudi et al. [16] have shown that the GMC method is unable to realize the transverse shear stress when the composite is loaded with global transverse strain. In order to address this problem, second order terms in the local coordinate are included in the displacement formulation of HFGMC method by Aboudi et al. [16].

Figure 2.1 shows the schematic multiscale modeling of HFGMC method. From the figure, it can be seen that:

- The structure at a global scale (Fig. 2.1(a)) is divided into the number of unit cells. If the repetition of any single unit cell in the two or three dimension space produces the same global structure, it is considered as a repeating unit cell (RUC). HFGMC can also be extended for analysis the nonrepetitive unit cell in which the entire domain is discretized in the subcells.

- RUC, identified in the Fig. 2.1(b), are further divided into $N_\beta \times N_\gamma$ subcells. The dimension
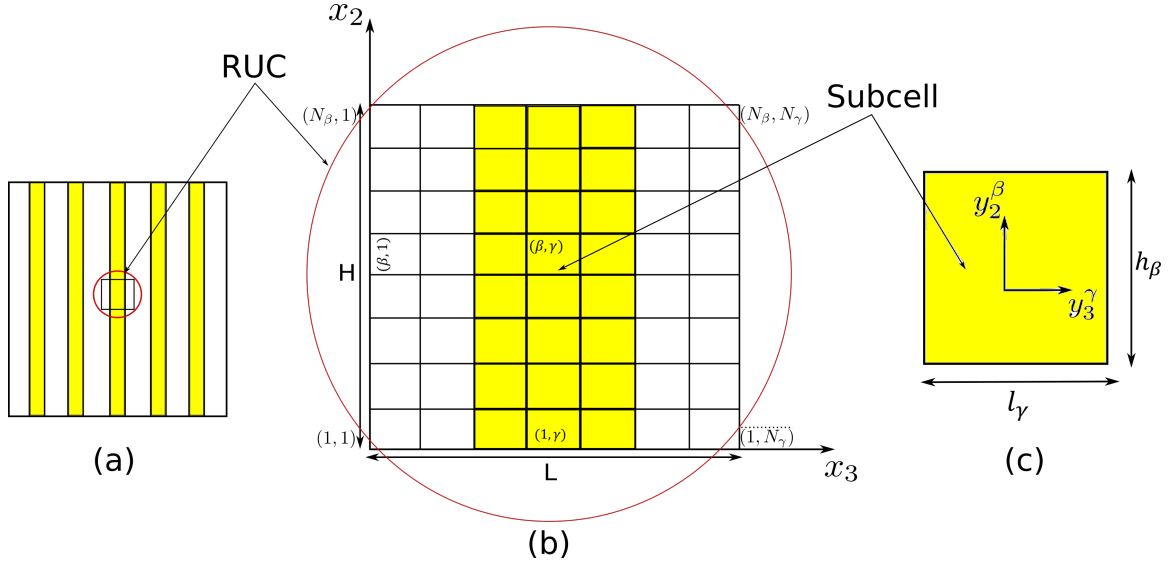
Figure 2.1: Multi-scale modeling in HFGMC analysis

of the RUC is taken H as a height, and L as a length and x_2 and x_3 is a global coordinate system.

- Each subcell has a dimension of h_β and l_γ. The local coordinate system (y_2^β, y_3^γ) is placed in the center of the subcell as shown in Fig. 2.1(c).

In the present work single fiber composite is analyzed in two dimension with the HFGMC formulation. However several other application of HFGMC are reported in the literature by Haj-Ali & Aboudi [17, 18].

The novelty of the present work lies in using the progressive damage analysis (PDA) coupled with the HFGMC framework. Re-equilibrium is required after each degradation and the analysis is highly non linear in nature. Aboudi et al [16] have only focused on the material non linearity and not on the PDA where the non linearity comes due to the degradation in the material properties. Greater details on the PDA can be found in Chapter 3.

2.2 HFGMC formulation

The detailed discussion on the HFGMC methodology is available in Aboudi et al [16]. For the completeness of the work, the HFGMC formulation is presented in the subsequent paragraphs to lay the foundation of PDA which is discussed in the Chapter 3.

2.2.1 Displacement vector in HFGMC framework

The basic displacement equation used in the HFGMC framework is derived from the expansion of the Eq. (2.3).

$$u^{\beta\gamma} = \bar{\epsilon}.X + \sum_{m=0}^{M}\sum_{n=0}^{N}\mathbf{w}_{(mn)}P_m\left(r\right)P_n\left(s\right) \tag{2.3}$$

In Eq. (2.3), $\bar{\epsilon}$ is the global externally applied strain, $P_m(r)$ and $P_n(s)$ are the Legendre polynomials, M and N are the maximum orders required in the displacement polynimials. For the HFGMC formulation, M and N are taken to be equal to 2 each such that the displacement equation is quadratic in the coordinate r and s which are uniform parametric coordinates. $\mathbf{w}_{(mn)}$ is the coefficient variable vector. The standard complete expansion of the Eq. (2.3) gives the Eq. (2.4).

$$u^{\beta\gamma} = \bar{\epsilon}.X + \mathbf{w}_{(00)} + r\mathbf{w}_{(10)} + s\mathbf{w}_{(01)} + rs\mathbf{w}_{(11)} + \frac{1}{2}\mathbf{w}_{(20)}\left(3r^2 - 1\right) + \frac{1}{2}\mathbf{w}_{(02)}\left(3s^2 - 1\right) \qquad (2.4)$$

The detailed expansion of the Eq. (2.3) is given in appendix A.

It is assumed that the product between the two Legendre Polynomial in the Eq. (2.3) is a dot product. When the orthogonal discretization of RUC is used, the term $\mathbf{w}_{11}$ goes to zero as it involves the dot product of two perpendicular vectors. Thus the bilinear term $y_2y_3\mathbf{w}_{(11)}$ does not exist in the incomplete displacement formulation of HFGMC with orthogonal discretization of RUC. Hence the displacement equation of the subcell in HFGMC methodology is given as:

$$u^{\beta\gamma} = \bar{\epsilon}.X + \mathbf{w}_{(00)}^{\beta\gamma} + y_2^{\beta}\mathbf{w}_{(10)}^{\beta\gamma} + y_3^{\gamma}\mathbf{w}_{(01)}^{\beta\gamma} + \frac{1}{2}\left(3y_2^{\beta2} - \frac{h_\beta^2}{4}\right)\mathbf{w}_{(20)}^{\beta\gamma} + \frac{1}{2}\left(3y_3^{\gamma2} - \frac{l_\gamma^2}{4}\right)\mathbf{w}_{(02)}^{\beta\gamma} \qquad (2.5)$$

where y_2^{β} and y_3^{γ} are the local coordinate axes, centered at the center of a subcell. h_β and l_γ are the height and the width of the subcell respectively (see Figure 2.1(c)).

For two different discretization illustrated in Fig. 2.2, displacement Eqs. (2.4) and (2.5) are differ-

a) Orthogonal
discretization

b) Non-orthogonal
discretization
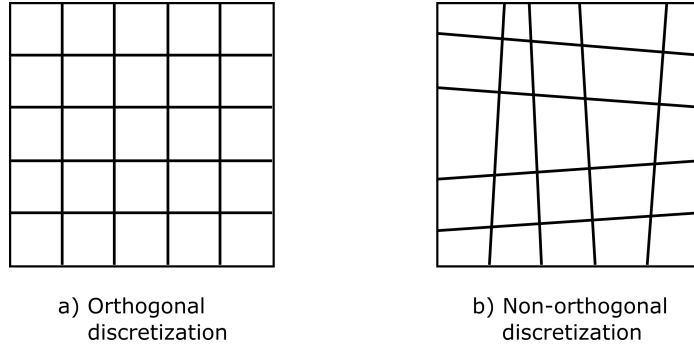
Figure 2.2: Multi-scale modeling in HFGMC analysis

ent. However in the current framework the discretization of single fiber composite is orthogonal in nature (similar to Fig. 2.2(a)). Hence Eq. (2.5) is followed. It is same as Eq. (2.4). By doing so, the degrees of freedom are limited to 15 as compared to 18. Thus less computation is required for less number of unknowns.

In Sections 2.2.2–2.2.8, derivations are performed to calculate the unknown displacement microvariable $\mathbf{w}_{(mn)}$.

2.2.2 Strain vector at each subcell

The average strain vector $\bar{\epsilon}^{\beta\gamma}$ is written in the Voigt notation [1] in the equation given below:

$$\bar{\epsilon}^{\beta\gamma} = \left(\epsilon_{11}, \epsilon_{22}, \epsilon_{33}, 2\epsilon_{23}, 2\epsilon_{13}, 2\epsilon_{12}\right)^{\beta\gamma} \qquad (2.6)$$

11

The finite strain tensor is given as:

$$\epsilon_{ij} = \frac{1}{2} \left(u_{i,j} + u_{j,i} + u_{k,i}u_{k,j} \right) \tag{2.7}$$

In the HFGMC analysis, small strain assumption is made [19] such that it can be derived from displacement Eq. (2.5) with help the of differentials given below:

$$\epsilon_{ij} = \frac{1}{2} \left(u_{i,j} + u_{j,i} \right) \tag{2.8}$$

Above strain term can be expanded for all the six strain components. Strain terms comes out to be:

$$\epsilon^{\beta\gamma} = \bar{\epsilon} + p_{(10)}\mathbf{w}^{\beta\gamma}_{(10)} + p_{(01)}\mathbf{w}^{\beta\gamma}_{(01)} + p_{(20)}\mathbf{w}^{\beta\gamma}_{(20)}y_2{}^{\beta} + p_{(02)}\mathbf{w}^{\beta\gamma}_{(02)}y_3{}^{\gamma} \tag{2.9}$$

where,

$$p_{(01)} = \begin{bmatrix} 0 & 0 & 0 \\ 0 & 0 & 0 \\ 0 & 0 & 1 \\ 0 & 0 & 0 \\ 1 & 0 & 0 \\ 0 & 1 & 0 \end{bmatrix} \qquad p_{(10)} = \begin{bmatrix} 0 & 0 & 0 \\ 0 & 1 & 0 \\ 0 & 0 & 0 \\ 1 & 0 & 0 \\ 0 & 0 & 0 \\ 0 & 0 & 1 \end{bmatrix} \tag{2.10}$$

also

$$p_{(20)} = 3p_{(10)} \qquad p_{(02)} = 3p_{(01)} \tag{2.11}$$

In Eq. (2.9), $\bar{\epsilon}$ is the global externally applied strain.

2.2.3 Average strain

The average strain in HFGMC analysis is derived from the Eq. (2.9) itself. The linear terms $p_{(20)}\mathbf{w}^{\beta\gamma}_{(20)}y_2{}^{\beta}$ and $p_{(02)}\mathbf{w}^{\beta\gamma}_{(02)}y_3{}^{\gamma}$ are zero in the average sense about the center of the subcell. Thus the average strain equation becomes:

$$\bar{\epsilon}^{\beta\gamma} = \bar{\epsilon} + p_{(01)}\mathbf{w}^{\beta\gamma}_{(01)} + p_{(10)}\mathbf{w}^{\beta\gamma}_{(10)} \tag{2.12}$$

In the Eq. (2.12) $\bar{\epsilon}$ refers to average strain that has been applied externally. The Eq. (2.12) is expressed in incremental form, that is used in the numerical implementation of HFGMC analysis. Strain influence matrix $\mathbf{B}^{\beta\gamma}$ is taken out of the expression.

$$\Delta\bar{\epsilon}^{\beta\gamma} \equiv \mathbf{B}^{\beta\gamma}\Delta\bar{\epsilon} = \left[\mathbf{I} + P_{(10)}\hat{\mathbf{D}}^{\beta\gamma}_{(10)} + P_{(01)}\hat{\mathbf{D}}^{\beta\gamma}_{(01)} \right]\Delta\bar{\epsilon} \tag{2.13}$$

where $\mathbf{I}$ is the identity matrix, $\hat{\mathbf{D}}^{\beta\gamma}_{(01)}\Delta\bar{\epsilon} = \mathbf{w}^{\beta\gamma}_{(01)}$ and $\hat{\mathbf{D}}^{\beta\gamma}_{(10)}\Delta\bar{\epsilon} = \mathbf{w}^{\beta\gamma}_{(10)}$

2.2.4 Average stress

The expression of stress is assumed to follow linear expansion in the local coordinate system [16]. Stress vector is defined in the Eq. (2.14) .

$$\sigma^{\beta\gamma} = \bar{\sigma}^{\beta\gamma} + \sigma^{\beta\gamma}_{(10)} y_2^{\beta} + \sigma^{\beta\gamma}_{(01)} y_3^{\gamma} \tag{2.14}$$

Where $\bar{\sigma}^{\beta\gamma}$ is the average stress in the cell $\beta\gamma$ and the stress per unit length $\sigma^{\beta\gamma}_{(mn)}$ can be found out using the total stresses that are determined at the stress integration points (see Fig. 2.3).

$$\sigma^{\beta\gamma}_{(10)} = \frac{1}{h_\beta}(\sigma^{\beta\gamma_1} - \sigma^{\beta\gamma_3}) \tag{2.15}$$

$$\sigma^{\beta\gamma}_{(01)} = \frac{1}{l_\gamma}(\sigma^{\beta\gamma_2} - \sigma^{\beta\gamma_4}) \tag{2.16}$$

The value of stress per unit length $\sigma^{\beta\gamma}_{(mn)}$, can also be calculated with the help of stress moments,
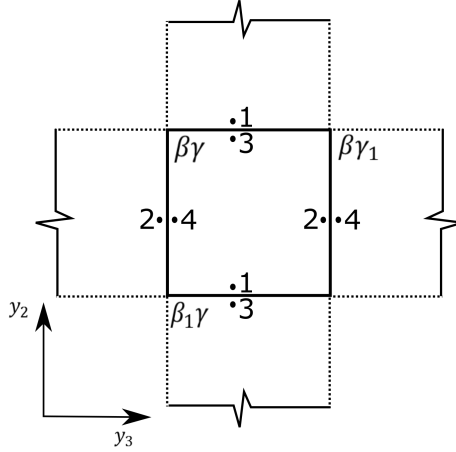
Figure 2.3: Stress integration at subcell interface

but the above form (Eqs. (2.15) and (2.16)) is preferred for easy numerical implementation.

2.2.5 Equilibrium equation

An equilibrium equation can be written as $\nabla.\sigma = 0$. For static analysis the dynamic terms involved in the equilibrium equations are neglected [20]. For HFGMC analysis, the equilibrium equation is written in the matrix form as shown in the Eq. (2.17) below:

$$r_2 \sigma^{\beta\gamma}_{(10)} + r_3 \sigma^{\beta\gamma}_{(01)} = 0 \tag{2.17}$$

In the Eq. (2.17) $r_2 = p_{10}^T$ and $r_3 = p_{01}^T$. Here T represents transpose.

2.2.6 Incremental form of constitutive relation

The incremental form of the constitutive relation, for the material available in the subcell $(\beta\gamma)$, is given by the equation:

$$\Delta\sigma^{\beta\gamma} = C^{\beta\gamma}\Delta\epsilon^{\beta\gamma} \tag{2.18}$$

$C^{\beta\gamma}$ is selected considering linear or nonlinear behavior of the material present in the subcell. The incremental form of the stress in Eq. (2.14) is given as:

$$\Delta\sigma^{\beta\gamma} = \Delta\bar{\sigma}^{\beta\gamma} + \Delta\sigma_{(10)}^{\beta\gamma}y_2^{(\beta)} + \Delta\sigma_{(01)}^{\beta\gamma}y_3^{(\gamma)} \tag{2.19}$$

Pre-multiplying $C^{\beta\gamma}$ on both the sides of the incremental form of the Eq. (2.9), following equation is obtained:

$$C^{\beta\gamma}\Delta\epsilon^{\beta\gamma} =$$
$$C^{\beta\gamma}\Delta\bar{\epsilon} + C^{\beta\gamma}p_{(10)}\Delta\mathbf{w}_{(10)}^{\beta\gamma}+$$
$$C^{\beta\gamma}p_{(01)}\Delta\mathbf{w}_{(01)}^{\beta\gamma} + C^{\beta\gamma}p_{(20)}\Delta\mathbf{w}_{(20)}^{\beta\gamma}y_2^{\beta} + C^{\beta\gamma}p_{(02)}\Delta\mathbf{w}_{(02)}^{\beta\gamma}y_3^{\gamma} \tag{2.20}$$

As the L.H.S of the Eqs. (2.19) and (2.20) are same, their R.H.S are be compared to give the incremental form of stresses shown in Eq. (2.21).

$$\begin{array}{rcl} \Delta\bar{\sigma}^{\beta\gamma} & = & C^{\beta\gamma}\Delta\bar{\epsilon} + C^{\beta\gamma}p_{(01)}\Delta\mathbf{w}_{(01)}^{\beta\gamma} + C^{\beta\gamma}p_{(10)}\Delta\mathbf{w}_{(10)}^{\beta\gamma} \\ \Delta\sigma_{(10)}^{\beta\gamma} & = & C^{\beta\gamma}p_{(20)}\Delta\mathbf{w}_{(20)}^{\beta\gamma} \\ \Delta\sigma_{(01)}^{\beta\gamma} & = & C^{\beta\gamma}p_{(02)}\Delta\mathbf{w}_{(02)}^{\beta\gamma} \end{array} \tag{2.21}$$

Eq. (2.17) can be written in incremental form as:

$$r_2 C^{\beta\gamma}p_{(20)}\Delta\mathbf{w}_{(20)}^{\beta\gamma} + r_3 C^{\beta\gamma}p_{(02)}\Delta\mathbf{w}_{(02)}^{\beta\gamma} = 0 \tag{2.22}$$

In the compact form, the increment form of the equilibrium equation is thus derived as:

$$Q_{2(20)}^{\beta\gamma}\Delta\mathbf{w}_{(20)}^{\beta\gamma} + Q_{3(02)}^{\beta\gamma}\Delta\mathbf{w}_{(02)}^{\beta\gamma} = 0 \tag{2.23}$$

where $Q_{i(mn)}^{\beta\gamma} \equiv r_i C^{\beta\gamma}p_{(mn)}$ for $(mn) \neq (00)$ and $Q_{i(00)}^{\beta\gamma} \equiv r_i C^{\beta\gamma}$

2.2.7 Traction and displacement continuity

To enforce the displacement and the traction continuity between the subcells, Eqs. (2.24)–(2.27) are presented. These continuity equations are defined along the interface between two neighboring subcells as follows:

For the Eqs. (2.24) and (2.25), the continuity equations for displacement and continuity are defined on the boundary with normal in y_3 direction.

$$\int_{\frac{-h_\beta}{2}}^{\frac{h_\beta}{2}} \left[u^{\beta\gamma}\big|_{y_3^{(\gamma)}=\frac{l_\gamma}{2}} - u^{(\beta\gamma_1)}\big|_{y_3^{(\gamma_1)}=\frac{l_{\gamma_1}}{2}} \right] dy_2^{(\beta)} = 0 \tag{2.24}$$

$$\int_{-\frac{h_\beta}{2}}^{\frac{h_\beta}{2}} \left[r_3 \sigma^{(\beta\gamma)} \big|_{y_3^{(\gamma)} = -\frac{l_\gamma}{2}} - r_3 \sigma^{(\beta\gamma_1)} \big|_{y_3^{(\gamma_1)} = -\frac{l_{\gamma_1}}{2}} \right] dy_2^{(\beta)} = 0 \tag{2.25}$$

For the Eqs. (2.26) and (2.27), the continuity equations for displacement and continuity are defined on the boundary with normal in y_2 direction. For directions y_2 and y_3, see Fig. 2.1(c).

$$\int_{-\frac{l_\gamma}{2}}^{\frac{l_\gamma}{2}} \left[u^{\beta\gamma} \big|_{y_2^{(\beta)} = \frac{h_\beta}{2}} - u^{(\beta_1\gamma)} \big|_{y_2^{(\beta_1)} = \frac{h_{\beta_1}}{2}} \right] dy_3^{(\gamma)} = 0 \tag{2.26}$$

$$\int_{-\frac{l_\gamma}{2}}^{\frac{l_\gamma}{2}} \left[r_2 \sigma^{(\beta\gamma)} \big|_{y_2^{(\beta)} = -\frac{h_\beta}{2}} - r_2 \sigma^{(\beta_1\gamma)} \big|_{y_2^{(\beta_1)} = -\frac{h_{\beta_1}}{2}} \right] dy_3^{(\gamma)} = 0 \tag{2.27}$$

Above equations are further simplified after putting the value of displacement and traction in the incremental form. The result yields following four equations.

$$\left[\Delta\mathbf{w}_{(00)}^{(\beta\gamma)} + \frac{l_\gamma}{2} \Delta\mathbf{w}_{(01)}^{(\beta\gamma)} + \frac{l_\gamma^2}{4} \Delta\mathbf{w}_{(02)}^{(\beta\gamma)} \right] - \left[\Delta\mathbf{w}_{(00)}^{(\beta\gamma_1)} - \frac{l_{\gamma_1}}{2} \Delta\mathbf{w}_{(01)}^{(\beta\gamma_1)} + \frac{l_{\gamma_1}^2}{4} \Delta\mathbf{w}_{(02)}^{(\beta\gamma_1)} \right] = 0 \tag{2.28}$$

$$\left[\Delta\mathbf{w}_{(00)}^{(\beta\gamma)} - \frac{h_\beta}{2} \Delta\mathbf{w}_{(10)}^{(\beta\gamma)} + \frac{h_\beta^2}{4} \Delta\mathbf{w}_{(20)}^{(\beta\gamma)} \right] - \left[\Delta\mathbf{w}_{(00)}^{(\beta_1\gamma)} + \frac{h_{\beta_1}}{2} \Delta\mathbf{w}_{(10)}^{(\beta_1\gamma)} + \frac{h_{\beta_1}^2}{4} \Delta\mathbf{w}_{(20)}^{(\beta_1\gamma)} \right] = 0 \tag{2.29}$$

$$\begin{aligned}
\left[Q_{3(00)}^{(\beta\gamma_1)} - Q_{3(00)}^{(\beta\gamma)} \right] \Delta\bar{\epsilon} &= \left[Q_{3(10)}^{(\beta\gamma)} \Delta\mathbf{w}_{(10)}^{(\beta\gamma)} + Q_{3(01)}^{(\beta\gamma)} \Delta\mathbf{w}_{(01)}^{(\beta\gamma)} + \frac{l_\gamma}{2} Q_{3(02)}^{(\beta\gamma)} \Delta\mathbf{w}_{(02)}^{(\beta\gamma)} \right] \\
&\quad - \left[Q_{3(10)}^{(\beta\gamma_1)} \Delta\mathbf{w}_{(10)}^{(\beta\gamma_1)} + Q_{3(01)}^{(\beta\gamma_1)} \Delta\mathbf{w}_{(01)}^{(\beta\gamma_1)} - \frac{l_{\gamma_1}}{2} Q_{3(02)}^{(\beta\gamma_1)} \Delta\mathbf{w}_{(02)}^{(\beta\gamma_1)} \right]
\end{aligned} \tag{2.30}$$

$$\begin{aligned}
\left[Q_{2(00)}^{(\beta_1\gamma)} - Q_{2(00)}^{(\beta\gamma)} \right] \Delta\bar{\epsilon} &= \left[Q_{2(10)}^{(\beta\gamma)} \Delta\mathbf{w}_{(10)}^{(\beta\gamma)} + Q_{2(01)}^{(\beta\gamma)} \Delta\mathbf{w}_{(01)}^{(\beta\gamma)} - \frac{h_\beta}{2} Q_{2(20)}^{(\beta\gamma)} \Delta\mathbf{w}_{(20)}^{(\beta\gamma)} \right] \\
&\quad - \left[Q_{2(10)}^{(\beta_1\gamma)} \Delta\mathbf{w}_{(10)}^{(\beta_1\gamma)} + Q_{2(01)}^{(\beta_1\gamma)} \Delta\mathbf{w}_{(01)}^{(\beta_1\gamma)} + \frac{h_{\beta_1}}{2} Q_{2(20)}^{(\beta_1\gamma)} \Delta\mathbf{w}_{(20)}^{(\beta_1\gamma)} \right]
\end{aligned} \tag{2.31}$$

Eq. (2.23) and Eqs.(2.28)-(2.31) are combined together to form the system of linear equations. It has been discussed in the Section 2.2.8.

2.2.8 System of equations and unknowns

The displacement vector in the HFGMC formulation consists of five unknown vectors: $\Delta\mathbf{w}_{(10)}^{(\beta\gamma)}$, $\Delta\mathbf{w}_{(01)}^{(\beta\gamma)}$, $\Delta\mathbf{w}_{(00)}^{(\beta\gamma)}$, $\Delta\mathbf{w}_{(20)}^{(\beta\gamma)}$, $\Delta\mathbf{w}_{(02)}^{(\beta\gamma)}$. These five unknown vector are combined together to form one unknown vector $\Delta X^{(\beta\gamma)}$:

$$\Delta X^{(\beta\gamma)} = \left\{ \Delta\mathbf{w}_{(10)}^{(\beta\gamma)}, \Delta\mathbf{w}_{(01)}^{(\beta\gamma)}, \Delta\mathbf{w}_{(00)}^{(\beta\gamma)}, \Delta\mathbf{w}_{(20)}^{(\beta\gamma)}, \Delta\mathbf{w}_{(02)}^{(\beta\gamma)} \right\} \tag{2.32}$$

Each $\Delta\mathbf{w}$ vector consists of three unknown along 1, 2 and 3 component of the coordinate system. Counting the contribution of every $\Delta\mathbf{w}$, the length of the unknown vector $\Delta X^{\beta\gamma}$ is 15 for a subcell $\beta\gamma$.

Using the Eq. (2.23) and Eqs.(2.28)-(2.31), system of linear equations of the form $AX = B$ is formed.

This system of equations consists of five equations and five unknowns vectors for a single subcell. A global set of equations is obtained by assembling all the equations obtained in the process. For the number of subcells equal to $N_\beta \times N_\gamma$, the number of unknowns become $15 \times N_\beta \times N_\gamma$.

$$M_G \Delta X - N_G \Delta \epsilon = 0 \tag{2.33}$$

In the Eq. (2.33) M_G and N_G are the global matrix obtained after assembling individual subcell's M and N matrices. Such M and N vectors are obtained from the set of the traction and the displacement continuity equations along with the equilibrium equation for every subcell. They have been given such a form to take out unknown vector ΔX and form the linear system of equations. Matrices shown below gives the value of M and N matrix.

$$M_1^{(\beta\gamma)} = \begin{bmatrix} Q_{2(10)} & Q_{2(01)} & 0 & -\frac{h_\beta}{2}Q_{2(20)} & 0 \\ Q_{3(10)} & Q_{3(01)} & 0 & 0 & -\frac{l_\gamma}{2}Q_{3(02)} \\ 0 & 0 & 0 & Q_{2(20)} & Q_{3(02)} \\ -\frac{h_\beta}{2}I & 0 & I & \frac{h_\beta^2}{4}I & 0 \\ 0 & \frac{l_\gamma}{2}I & I & 0 & \frac{l_\gamma^2}{4}I \end{bmatrix}^{\beta\gamma}$$

$$M_2^{(\beta_1\gamma)} = \begin{bmatrix} -Q_{2(10)} & -Q_{2(01)} & 0 & -\frac{h_{\beta_1}}{2}Q_{2(20)} & 0 \\ 0 & 0 & 0 & 0 & 0 \\ 0 & 0 & 0 & 0 & 0 \\ -\frac{h_{\beta_1}}{2}I & 0 & -I & -\frac{h_{\beta_1}^2}{4}I & 0 \\ 0 & 0 & 0 & 0 & 0 \end{bmatrix}^{(\beta_1\gamma)}$$

$$M_3^{(\beta\gamma_1)} = \begin{bmatrix} 0 & 0 & 0 & 0 & 0 \\ -Q_{3(10)} & -Q_{3(01)} & 0 & 0 & \frac{l_{\gamma_1}}{2}Q_{3(02)} \\ 0 & 0 & 0 & 0 & 0 \\ 0 & 0 & 0 & 0 & 0 \\ 0 & \frac{l_{\gamma_1}}{2}I & -I & 0 & \frac{l_{\gamma_1}^2}{4}I \end{bmatrix}^{(\beta\gamma_1)}$$

$$N_1^{(\beta\gamma)} = \begin{bmatrix} -Q_{2(00)} \\ -Q_{3(00)} \\ 0 \\ 0 \\ 0 \end{bmatrix}^{\beta\gamma} , \quad N_2^{(\beta_1\gamma)} = \begin{bmatrix} Q_{2(00)} \\ 0 \\ 0 \\ 0 \\ 0 \end{bmatrix}^{\beta_1\gamma} \quad \text{and} \quad N_3^{(\beta\gamma_1)} = \begin{bmatrix} 0 \\ Q_{3(00)} \\ 0 \\ 0 \\ 0 \end{bmatrix}^{\beta\gamma_1}$$

Rearranging the Eq. (2.33), following equation is obtained:

$$\Delta X = M_G^{-1}(N_G \Delta \epsilon) \tag{2.34}$$

16

2.2.9 Residual vector

Residue vector is required for calculating error involved in the iterative solvers. It is further required to follow Newton Raphson iterative scheme. Residual vector in its incremental form $\Delta R^{\beta\gamma}$ has been defined as:

$$\Delta R^{\beta\gamma} \equiv \{\Delta R_\sigma, \Delta R_E, \Delta R_u\} \tag{2.35}$$

In the Eq. (2.35) ΔR_σ represents the residue based on two traction continuity expressions given by Eqs. (2.30) & (2.31). Other terms ΔR_E and ΔR_u represents residue for equilibrium Eq. (2.23) and displacement continuity Eqs. (2.28) and (2.29) respectively. Thus

$$\Delta R^{\beta\gamma} \equiv \{M_1^{\beta\gamma}\Delta X^{\beta\gamma} - N_1^{\beta\gamma}\Delta\bar{\epsilon}\} + \{M_2^{(\beta_1\gamma)}\Delta X^{(\beta_1\gamma)} - N_2^{(\beta_1\gamma)}\Delta\bar{\epsilon}\} + \{M_3^{(\beta\gamma_1)}\Delta X^{(\beta\gamma_1)} - N_3^{(\beta\gamma_1)}\Delta\bar{\epsilon}\} \tag{2.36}$$

The residue for numerical implementation of HFGMC is calculated with the help of total stresses calculated at the stress integration points. In order to do so, for a particular subcell, total residual vector is calculated in the integral form rather than incremental one as defined in Eq. (2.36). It has been calculated at stress integration points shown in the Fig. 2.3. It is given as:

$$R^{(\beta\gamma)} = \begin{bmatrix} r_2\sigma^{(\beta\gamma)_1} - r_2\sigma^{(\beta_1\gamma)_3} \\ r_3\sigma^{(\beta\gamma)_2} - r_3\sigma^{(\beta\gamma_1)_4} \\ r_2\sigma^{(\beta\gamma)}_{(10)} - r_3\sigma^{(\beta\gamma)}_{(01)} \\ 0 \\ 0 \end{bmatrix} \tag{2.37}$$

Once the residue is obtained, the Newton Raphson iterative scheme is applied. The process is as explained below:

Initially the residual vector is calculated between the current and the previous iteration solution. If the norm of the residue is less than the allowable tolerance of 10^{-5} than the solution of current step is accepted, otherwise correction for micro-variable is computed with the help of the Jacobian. The micro variables are updated with the corrections based on Jacobian calculations.

2.3 Homogenization of properties

Using HFGMC, both local and averaged stress-strain field are obtained. The local strain field in the RUC is related to globally applied homogenized strain field with the help of strain influence matrix $\mathbf{B}$, as shown in the Eq. (2.38). Here Δ denotes the incremental form of strain.

$$\Delta\bar{\epsilon}^{\beta\gamma} = \mathbf{B}\Delta\bar{\epsilon} \tag{2.38}$$

Further to find the stress field, the constitutive matrix of individual subcell is used in the following Eq. (2.39). Here H and L are the dimensions of RUC, $\mathbf{C}^{\beta\gamma}$ is the stiffness tensor of individual subcell, and h_β and l_γ are the dimensions of subcell.

$$\Delta\bar{\sigma} = \frac{1}{HL}\sum_{\gamma=1}^{N_\gamma}\sum_{\beta=1}^{N_\beta} h_\beta l_\gamma \mathbf{C}^{\beta\gamma}\mathbf{B}^{\beta\gamma}\Delta\bar{\epsilon} \tag{2.39}$$

17

Expression of $\mathbf{B}^{\beta\gamma}$ is obtained from the Eq. (2.13).

Using Eq. (2.39) one can find the effective stress update. Eqs. (2.3)–(2.39) completes the derivation of HFGMC formulation. Later in the Chapter 3, HFGMC methodology is coupled with damage detection and damage modeling to form the PDA. Further the parameters h_β, l_γ, H, L and $\mathbf{C}^{\beta\gamma}$ required in the Eq. (2.39) are detailed in the Sections 4.2.3 and 4.3.3.

Chapter 3

Methodology

Progressive damage analysis

Progressive damage analysis (PDA) [21] involves the detailed study of damage initiation, evaluation till final failure. PDA comprise of three steps. These are given in the schematic Fig. 3.1:

- Stress Analysis

- Damage Analysis

- Damage Modeling
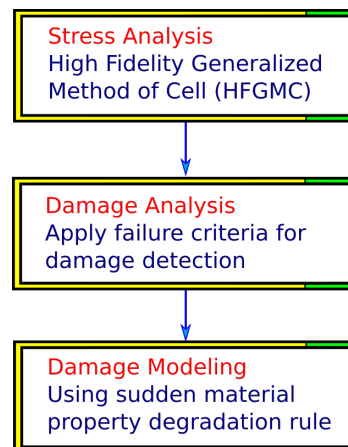
Figure 3.1: Basic steps involved in PDA

Current chapter contains the thorough explanation of all the three steps of PDA. Stress analysis is discussed in Section 3.1. In the Section 3.2, models for damage initiation and evaluation are discussed. Section 3.3 gives the information on the damage modeling aspect of the PDA. Progressive damage analysis have been performed numerically with the help of the home grown code devised in the Fortran fixed format. Structural outline of the code is explained in Section 3.4.

3.1   Stress analysis

Stress analysis is carried out using the HFGMC methodology to effectively capture the stress gradients present at the fiber/matrix interface. It is possible as the HFGMC method employs higher order terms in the displacement equation which helps in obtaining the local effects generated by composite microstructure. The detailed description of HFGMC methodology is available in Chapter 2.

3.1.1   Composite modeling for stress analysis with HFGMC method

Basic parameter are required to be preset for using the HFGMC method. These are:

- The single fiber composite (SFC) structure has been discretized into subcell. Each subcell is identified by $\beta\gamma$ index.

- Dimension of each sucell is h_β and l_γ. Discretization in HFGMC can be both regular and adaptive. In the former discretization, dimension of each subcell is identical to the other while in the later one different subcells have different dimensions. For the present case, only regular discretization has been used.

- The constitutive law is defined for every fiber and matrix subcell. Both fiber/matrix follow isotropic constitutive law at subcell level.

- Effective properties are calculated to evaluate homogenized stress strain behavior of the composite.

Using HFGMC stress analysis, stress value in each subcell is obtained using Eq. (2.39). The obtained stress value is used in the damage detection as described in subsequent section.

3.2   Damage detection

Several damage detection theories are available in the literature for composite materials [1, 22, 23, 24, 25]. For the effective property calculation of multi fiber composite, Multi Continuum Theory (MCT) is used. MCT provides a unified damage index over the fiber and the matrix subcells and it also considers the interaction effect between the fiber and the matrix subcell [24]. Detailed discussion of MCT is illustrated in the Section 3.2.2. Firstly, the MCT has been derived in detail, later, it has been used to device a failure criteria.
While analyzing the SFC for the successive fragmentation of the fiber, Maximum Principal Stress Theory is used [26]. It is discussed in the Section 3.2.1. Further the matrix is assumed to be ductile to take large strains such that it allows the progressive failure of the fiber. Thus no failure criteria is used for the matrix in the case of successive fiber fragmentation. Above mentioned assumptions have been further discussed in the Section 4.3.4.

3.2.1   Maximum Principle Stress Theory

Maximum principle stress criteria is used for the failure analysis of brittle material [23]. It assumes that the failure will occur in a material when the maximum principal stress in a complex stress

system reaches the elastic limit stress in a simple tension [27].

$$\sigma_1 = \sigma_{yp} \tag{3.1}$$

where σ_1 is the principal tensile stress. In the 2D state of stress, the principle stress σ_1 is obtained as

$$\sigma_1 = \frac{\sigma_x + \sigma_y}{2} + \sqrt{\left(\frac{\sigma_x - \sigma_y}{2}\right)^2 + \tau_{xy}^2} \tag{3.2}$$

Where σ_x and σ_y are the tensile stresses in the x and y direction respectively and τ_{xy} is the shear on the plane x in y direction.

3.2.2 Multi continuum theory (MCT)

The Representative Volume Element (RVE) concept is used in the derivation of the MCT theory. It is explained using the Fig. 3.2. The detailed literature on the RVE subject is available in Drugan [28] and Kanit et al [29]. RVE helps in determining the effective mechanical quantities of the continuum. RVE has reduced dimensions as compared to the global dimension of the body. Its dimensions are chosen to represent a statistically accurate microstructure.

Consider Fig. 3.2 that shows the hypothetical composite cross section in which the gray and the
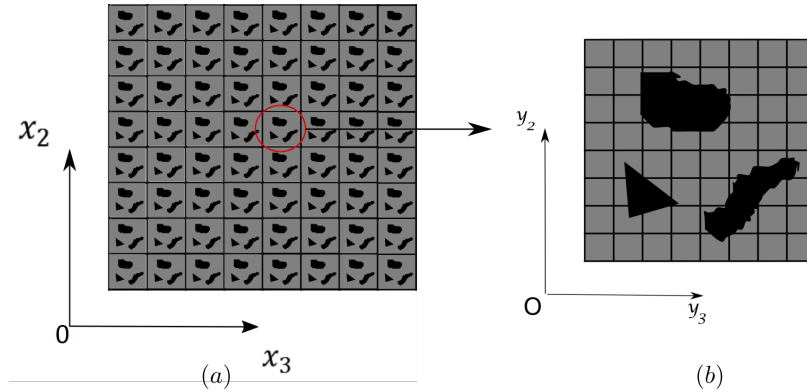
Figure 3.2: Composite and its RVE

black material are assumed as the matrix and the fiber respectively. The enlarged portion of the selected unit cell is presented in Fig. 3.2(b). The selected unit also represents a Repeating Unit cell (RUC) such that its repetition in two dimension form the structure given in Fig. 3.2(a). If the analysis of RUC with periodic boundary condition evaluates the effective mechanical quantities of the composite structure, then the RUC is also the representative volume element (RVE).

Subsequent paragraphs deals with the derivation of the basic concepts of MCT and its usage in determining damage criteria. It has been reviewed from the work of Hashin [30] and Mayes [24]. The literature available in Mayes [24] is first used in deriving the MCT, further Tsai and Wu failure criteria, present in Hashin [30], is used in obtaining the MCT damage criteria.

In the MCT, unknown strains in the matrix and the fiber are evaluated with the help of Eq. (3.11) and Eq. (3.12). To this end, the RVE concept is used. Corresponding to the composite structure,

21

having two phases (fiber and matrix), three volume averaged quantities are calculated (Eqs. (3.3)–(3.5)).

$$\sigma_f = \frac{1}{V_f} \int_{D_f} \sigma(\mathbf{x}) \, dV \tag{3.3}$$

$$\sigma_m = \frac{1}{V_m} \int_{D_m} \sigma(\mathbf{x}) \, dV \tag{3.4}$$

In the Eq. (3.3) and (3.4), V_f and V_m are volume of the fiber and the matrix respectively. $\sigma(\mathbf{x})$ is the stress value at the position $\mathbf{x}$. D_f and D_m are the respective domain over which the integration is carried out. If the material is considered to be a single continuum, then the value of average stress comes out to be

$$\sigma = \frac{1}{V} \int_{D} \sigma(\mathbf{x}) \, dV \tag{3.5}$$

Comparing the Eq. (3.3), (3.4) and (3.5), average value of stress over the RVE comes out to be

$$\sigma = \sigma_f \phi_f + \sigma_m \phi_m \tag{3.6}$$

Following the same procedure, the average strain value is

$$\epsilon = \epsilon_f \phi_f + \epsilon_m \phi_m \tag{3.7}$$

Note that ϕ_f and ϕ_m are the corresponding volume fractions of the fiber and the matrix. Using the constitutive law for each of the composite, fiber and matrix separately, the equations between stress and strain are given below:

$$\{\sigma\} = [C]\{\epsilon\} \tag{3.8}$$

$$\{\sigma_f\} = [C_f]\{\epsilon_f\} \tag{3.9}$$

$$\{\sigma_m\} = [C_m]\{\epsilon_m\} \tag{3.10}$$

Combining Eqs. (3.6)–(3.10) (simplified in appendix C), the expression for the matrix and the fiber strains are obtained as

$$\{\epsilon_m\} = (\phi_m[I] + \phi_f[A])^{-1}\{\epsilon\} \tag{3.11}$$

$$\{\epsilon_f\} = \frac{1}{\phi_f}(\{\epsilon\} - \phi_m\{\epsilon_m\}) \tag{3.12}$$

Here [A] is

$$[A] = -\frac{\phi_m}{\phi_f}([C] - [C_f])^{-1}([C] - [C_m]) \tag{3.13}$$

The stress and strain information produced by MCT criteria is used with the generalized failure criteria proposed by Tsai and Wu [30], to construct the MCT failure criteria. The generalized failure criteria is given as

$$F_i\sigma_i + F_{ij}\sigma_i\sigma_j = 1 \tag{3.14}$$

When the failure criteria in Eq. (3.14) is expanded and written in form of stress invariant, the Eq. (3.15) is obtained.

$$Z_1 I_1 + A_1 {I_1}^2 + Z_2 I_2 + A_2 {I_2}^2 + C_{12} I_1 I_2 + A_3 I_3 + A_4 I_4 = 1 \tag{3.15}$$

Invariants I_1, I_2, I_3 and I_4 are given below:

$$I_1 = \sigma_{11}$$
$$I_2 = \sigma_{22} + \sigma_{33}$$
$$I_3 = \sigma_{22}^2 + \sigma_{33}^2 + 2\sigma_{23}^2$$
$$I_4 = \sigma_{12}^2 + \sigma_{13}^2 \tag{3.16}$$

Assuming that there is no stress interaction between the fiber and the matrix, the term C_{12} is set to zero. Stress invariants I_1 and I_2 are the first order term in stress. The coefficient Z_1 and Z_2 are set to zero since linear terms are already considered in the basic derivation of MCT.

$$A_1 I_1{}^2 + A_2 I_2{}^2 + A_3 I_3 + A_4 I_4 = 1 \tag{3.17}$$

Two primary failure modes in composite are the fiber failure mode (rupture in tension or buckling in compression) and the matrix failure mode (matrix crack parallel to the fiber) [30]. Fig. 3.3 shows the failure planes for fiber and matrix modes. Fiber is in the $'1'$ direction. Matrix failure planes are $'12'$ and $'13'$ while the fiber failure plane is $'23'$. The two failure modes have been discussed in detail in the subsequent Sections 3.2.3 and 3.2.4.
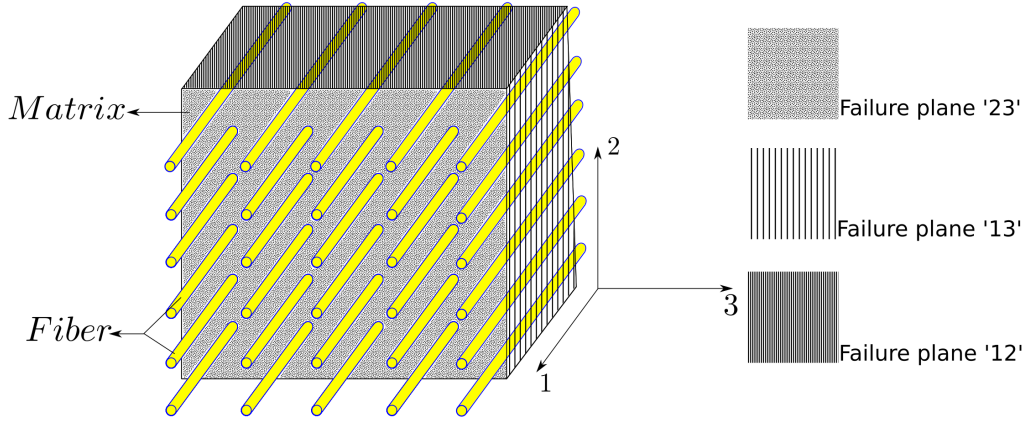
Figure 3.3: Primary failure mode planes in composite material

3.2.3 Fiber failure mode

The transverse failure of composite is matrix dominated. For considering the fiber strength only, all the invariants (see Eq. (3.16)) which are independent of stress in the plane $'1'$ have no effect on the failure equation. Thus the coefficients A_2 and A_3 in Eq. (3.17) are set to zero. Resulting failure equation is thus:

$$A_1^f \left(I_1^f \right)^2 + A_4^f I_4^f = 1 \tag{3.18}$$

Unknowns in the Eq. (3.18) are determined by considering their respective failure cases given in the Eqs. (3.19)–(3.21).

- Case of in-plane shear load only $\left(\sigma_{11}^f = 0\right)$

$$A_4^f = \frac{1}{S_{12}^f{}^2} \tag{3.19}$$

- Case of tensile load only $\left(\sigma_{11}^f > 0, \sigma_{11}^f = 0\right)$

$$A_4^{ft} = \frac{1}{S_{11}^{ft2}} \tag{3.20}$$

- Case of compressive load only $\left(\sigma_{11}^f < 0, \sigma_{11}^f = 0\right)$

$$A_4^{fc} = \frac{1}{S_{11}^{fc2}} \tag{3.21}$$

The S_{12}^f, S_{11}^{ft} and S_{11}^{fc} denotes the strength property in shear, tension and compression for fiber.

3.2.4   Matrix failure mode

Assuming the longitudinal failure of the composite is fiber dominated, A_1 has been set to zero in the Eq. (3.17). Then the criteria for matrix failure can be given as:

$$A_2^m (I_2^m)^2 + A_3^m I_3^m + A_4^m I_4^m = 1 \tag{3.22}$$

Constants for the matrix failure can be computed considering respective failure cases as given below:

- Transverse shear only $(\sigma_{11} = \sigma_{22} = \sigma_{33} = \sigma_{12} = 0)$

$$A_3^m = \frac{1}{2S_{23}^m{}^2} \tag{3.23}$$

- In-plane shear only $(\sigma_{11} = \sigma_{22} = \sigma_{33} = \sigma_{23} = 0)$

$$A_4^m = \frac{1}{2S_{12}^m{}^2} \tag{3.24}$$

- For transverse and compressive loads $(\sigma_{12} = \sigma_{23} = 0, (\sigma_{22} + \sigma_{33}) > or < 0)$

$$A_2^{mt} = \frac{1}{(S_{22}^{22mt} + S_{33}^{22mt})^2} \left(1 - \frac{(S_{22}^{22mt2} + S_{33}^{22mt2})}{2S_{23}^m{}^2}\right) \tag{3.25}$$

and

$$A_2^{mc} = \frac{1}{(S_{22}^{22mc} + S_{33}^{22mc})^2} \left(1 - \frac{(S_{22}^{22mc2} + S_{33}^{22mc2})}{2S_{23}^m{}^2}\right) \tag{3.26}$$

The subscript '22' in above failure parameter is denoting the direction of applied load.

The S_{22}^{22mt}, S_{33}^{22mt} are the matrix tensile strength in the direction 2 and 3 respectively. S_{22}^{22mc}, S_{33}^{22mc} are the matrix compressive strength in the direction 2 and 3 respectively and S_{12}^{m} denotes the strength property in shear.

Failure criteria derived in the present section will be used in the damage detection in the Section 4.2 which details the effective property calculation of multi fiber composite (MFC). Information gathered in the Section 3.2 is further utilized in the subsequent section which comprises of the damage modeling aspect of PDA.

3.3   Damage modeling

In the Section 3.2, material subcell gets damaged when it is loaded beyond the strength limit. With the damage detection, it is necessary to degrade the stiffness and the strength properties of the subcell accordingly. It ensures that the damaged subcell does not take external load in the next analysis step of PDA. Sudden degradation and progressive degradation models are available in the literature for damage modeling [31, 32]. In the present work, sudden material property degradation rule has been used. Degradation coefficient has been kept equal to 99% for both the MFC (Section 4.2) analysis and the SFC fiber fragmentation test (Section 4.3). Since in both the analysis, the structure under study has been loaded longitudinaly in the fiber direction, only the Young Modulus E_{11} and the Poisson's ratio are degraded as per the sudden material property degradation rule given in literature [32, 33]. The procedure of stiffness degradation is common in both the SFC fiber fragmentation test and MFC analysis. In order to consider the strength dependency of the fiber on its fragment length (Section 4.3.2), one additional function of reassigning the fiber strength is used in the damage modeling of single fiber fragment.

3.4   Structural outline of PDA

The source code for the progressive damage analysis has been devised in the Fortran language. The format of the code has been kept fixed so that it can be utilized in the user subroutine feature of the commercially available finite element softwares. The working procedure of the code is classified into four modules. All of them have been listed below:

1. **Input data for the analysis**
   The code requires several parameter to be preset to conduct the PDA of a given structure. These parameters are broadly classified into five categories:

   (a) **Geometric parameter**: Dimensions of the cell and subcell are specified.

   (b) **Material property**: Stiffness and strength properties of the fiber and the matrix are given.

   (c) **Discretization**: Number of subcells are provided to discretize the geometry of the structure.

   (d) **Degradation coefficient**: Damaged subcells are degraded using the degradation coefficient.

   (e) **Solver options**: The choice of the solver for the linear system of equations is selected here.

2. **Stress analysis**

   External global strain is applied in an incremental fashion to carry out the stress analysis. In this stage the HFGMC methodology is applied. The current stage thus includes the procedure to solve the linear system of equations. Considering the optimization between computational speed and accuracy, the code currently provides the choice among three different solvers:

   (a) DGELSD routine available in the LAPACK library [34]

   (b) Parallel direct solver (PARDISO) included in the Intel math kernel library [35, 36]

   (c) Linear Iterative Solver (LIS) [37]

   Analysis of global stiffness matrix T_G shows that its a sparse matrix with most of its elements lying along and near its diagonal. Sparsity of T_G matrix encourages one to use sparse solvers. First solver is taken from $LAPACK$ library. It is named as $DGELSD$. Complete description of this subroutine can be found in the literature [38]. It gives the most accurate result but the computation time is also high. It takes 45 minutes to perform stress analysis, when the geometry is discretized in 45×45 subcells. Second solver is the parallel direct solver (Intel MKL Pardiso solver) which is 9 times faster than that of the first discussed solver but it looses its accuracy with increase in number of subcells. The third solver is the Linear Iterative Solver (LIS), which is fast as compared to the $DGELSD$ but it also looses its accuracy with increase in number of subcells. For the present code, it is advised to use the second solver upto 45×45 subcells as it is already included in Intel MKL library and easy to use as compared to LIS solver. Appendix B shows the solution strategy for the linear equation involved in HFGMC analysis and it also justify the use of sparse solvers.

3. **Damage detection**

   Fracture indices are used to quantify the damage in subcells. MCT criteria is applied for the damage detection of the subcell while conducting the SFC-RVE analysis. Application of MCT criteria provides unified fracture index for both the fiber and the matrix. For the damage detection in the fiber fragmentation test of SFC, the maximum principle stress criteria provides the fracture index for the fiber subcell.

4. **Damage modeling**

   A subcell is termed as damaged if its fracture index is greater than one. The stiffness of the damaged subcell is degraded in an ad hoc manner. In the effective property calculation of multi fiber composite and SFC fiber fragmentation test, the degradation factor is kept 99%.

The detailed flowchart is shown in Fig. 3.4. Study conducted in the Chapters 2 and 3 is used in the analysis performed in Chapter 4:

The Section 4.3 talks about the SFC fiber fragmentation test followed by the Section 4.3.3 to explain the numerical analysis of SFC. The strength of the individual fiber fragment is modeled based on the literature discussed in the Section 4.3.2. Further the effective property calculation of multi fiber composite based on the SFC-RVE concept is discussed in the Section 4.2.

HFGMC Stress analysis

Obtain discretization of SFC in $N_\beta \times N_\gamma$ number of subcells

Obtain strain influence matrix **B** to get the local strain field as $\Delta\bar{\epsilon}^{\beta\gamma} = \mathbf{B}^{\beta\gamma}\Delta\bar{\epsilon}$

Obtain the global average stress as $\Delta\bar{\sigma} = \frac{1}{HL}\sum_{\gamma=1}^{N_\gamma}\sum_{\beta=1}^{N_\beta} h_\beta l_\gamma \mathbf{C}^{\beta\gamma}\mathbf{B}^{\beta\gamma}\Delta\bar{\epsilon}$

Local stress field of each subcell is obtained as $\Delta\bar{\sigma}^{\beta\gamma} = \mathbf{C}^{\beta\gamma}\Delta\bar{\epsilon}^{\beta\gamma}$

Auxiliary routine:
Strength of broken fiber fragment is redefined with the help of Weibull Strength Distribution as $\frac{\sigma}{\sigma_0} = \left(\frac{l_0}{l}\right)^{\frac{1}{k}}$

* For SFC-RVE analysis failure of two-third of total subcell is the analysis completion mark

Start

Input parameters:
1. Geometry
2. Material property
3. Degradation parameter
4. Loading
5. Numer of subcells

Define SFC architecture

Assign subcell definition as a fiber or a matrix subcell

Begin PDM with redifined properties of failed subcells

Stress analysis

Damage detection

Damage modeling

*Analysis completion mark: Fiber reaches its critical length

No

Yes

Stop

MCT/Max. Principle Stress Criteria

Obtain fracture index for each subcell as $FI^{\beta\gamma} = \frac{\sigma^{\beta\gamma}}{X^{\beta\gamma}}$

$FI^{\beta\gamma} \geq 1$

No → No damage of subcell

Yes → Damage of subcell

Sudden Material property degradation

$FI^{\beta\gamma} \geq 1$

Yes → $d^{\beta\gamma} = 0.99$

No → $d^{\beta\gamma} = 0$

Redefine material properties as $\mathbf{C}^{\beta\gamma} = (1 - d^{\beta\gamma})\mathbf{C}^{\beta\gamma}$

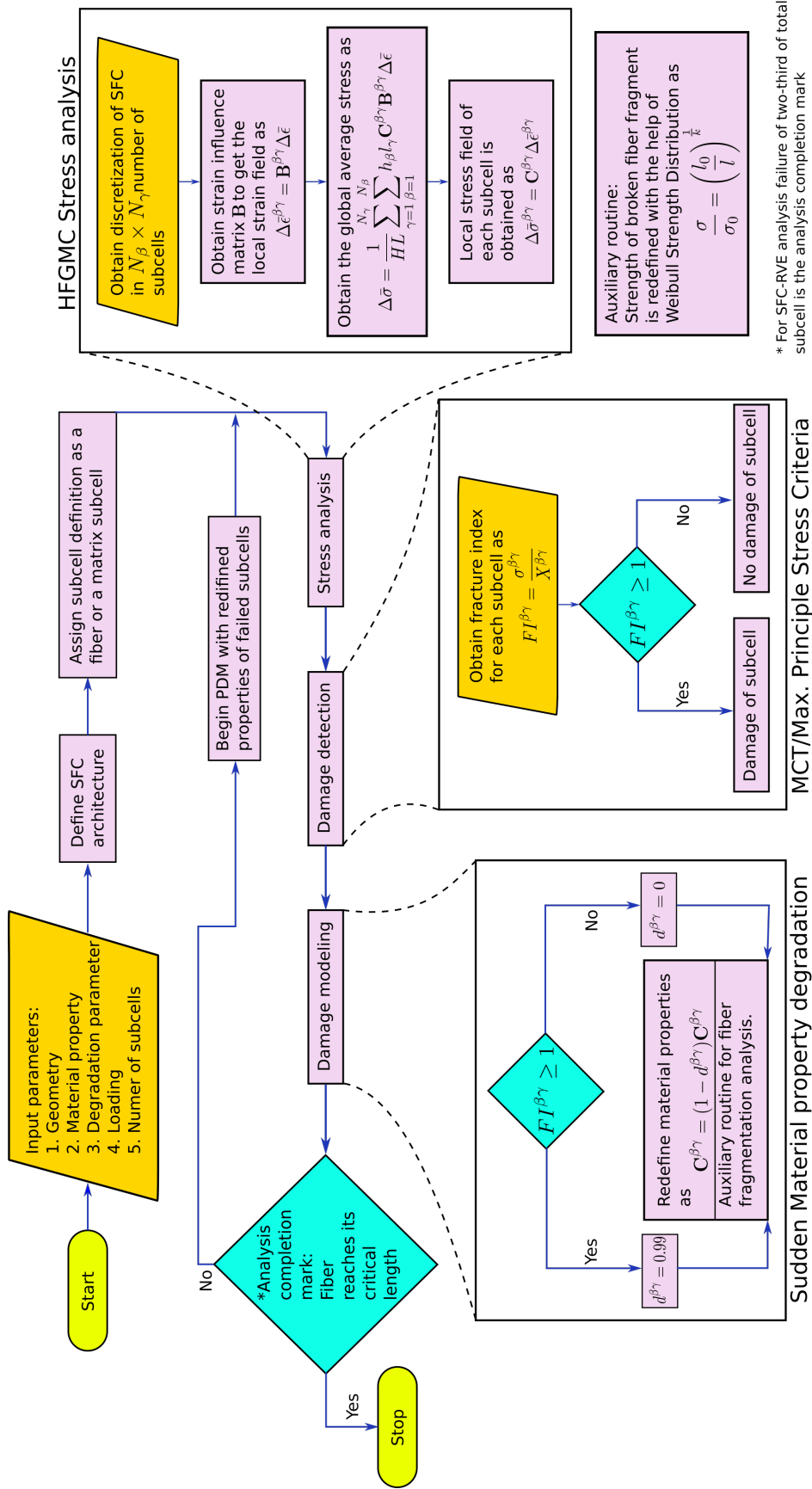Auxiliary routine for fiber fragmentation analysis.

Figure 3.4: Flowchart for SFC-RVE and SFC fiber fragmentation test

Chapter 4

Progressive damage analysis of single fiber composite

4.1 Introduction

Single Fiber Composite (SFC) is manufactured as a single fiber embedded in a cylindrical matrix [6, 26]. The interface between the fiber and the matrix is assumed to be perfectly bonded. It is used in the quantitative characterization of microscopic damages in the composites [39]. Experimental procedure of single fiber fragmentation test is explained in the literature [13, 26, 40].

Concepts discussed in the current chapter are broadly divided into two sections. Section 4.3 gives the detailed information on the fiber fragmentation test of the SFC while Section 4.2 presents the analysis required for the effective property calculation of multi fiber composites.

4.2 Effective property calculation of multi fiber composite

Multi fiber composite (MFC) has been studied with the SFC representative volume element (SFC-RVE) assuming that MFC can be modeled as SFC repeating unit cell (SFC-RUC) with periodic boundary condition (PBC). The aim of this analysis is to obtain the effective material properties through the size dependent framework and than compare it with the experimental findings and simplified analytical estimates. Similar to the fiber fragmentation test of SFC (Section 4.3), the PDA is adopted for the analysis. That is the HFGMC framework is used to carry out the stress analysis (Chapter 2 for detailed discussion). Damage detection is based on the multi continuum theory (Section 3.2.2). For the damage modeling, sudden material property degradation method is applied (see Section 3.3). From here onwards MFC is termed as SFC-RVE.

Individual fiber and matrix properties are given in Section 4.2.1. Material property of CFRP composite obtained from the experiment and the rule of mixture is presented in Section 4.2.2. Further the model of SFC-RVE for dimensions and boundary conditions are explained in Section 4.2.3. Assumptions for the analysis are stated in Section 4.2.4.

4.2.1 Material properties of fiber and matrix from experiment

The Carbon fiber reinforced polymer (CFRP) has been used for the analysis. Its properties have been taken from the work of Kashfuddoja & Ramji [41] where they had used Digital Image Correlation (DIC) technique to find the property values of CFRP composites. They are listed in the Table 4.1.

Table 4.1: Properties: Carbon fiber and epoxy resin

	Carbon fiber	Epoxy resin
Shear modulus (GPa)	$G_f = 88.461$	$G_m = 1.477$
Poisson's ratio	$\nu_f = 0.35$	$\nu_m = 0.34$
Volume fraction	$\phi_f = 0.33$	$\phi_m = 0.67$

4.2.2 Rule of mixture

In Section 5.1, the numerical results have been compared with both the experimental finding [41] and the analytical result based on the rule of mixture. In the rule of mixture, effective properties of the composites are found with the help of Eqs. (4.1) and (4.2) [42].

$$E_{11} = E_f \phi_f + E_m \phi_m \tag{4.1}$$

$$\nu_{12} = \nu_f \phi_f + \nu_m \phi_m \tag{4.2}$$

Refer Table 4.2 for experimental based and the rule of mixture based property values of CFRP composite.

Table 4.2: Longitudinal modulus (E_{11}) and In-plane Poisson's ratio (ν_{12})

	E_{11} (GPa)	ν_{12}
Experimental [41]	81.90	0.34
Rule of mixture	81.47	0.34

4.2.3 Model of SFC-RVE

The geometric model used in the present analysis of SFC-RVE is illustrated in Fig. 4.1. Fig. 4.1(a) shows the schematic of multi fiber composite (MFC). Fig. 4.1(b) shows the SFC-RVE taken out of the MFC structure for analysis. The SFC-RVE is discretized into $N_\beta \times N_\gamma$. For the discretization independent solution, the SFC-RVE is discretized in 30×30 subcells. Mesh increment studies shows that the analysis solution repeats itself with the discretization of 15×15, 30×30 and 45×45. The global coordinate system $x_2 - x_3$ for the SFC-RVE has been placed at the bottom left corner (origin $(0, 0)$). Fiber dimension is taken as 7.5 μm in diameter. Inter fiber distance in the MFC is chosen to be 15 μm and hence the matrix width is 7.5 μm on either side of the fiber. Length of the fiber is kept same as a width of the RVE. PBC exists at the four boundaries of the SFC-RVE.

The model shown in the Fig. 4.1, is loaded with the longitudinal strain ϵ in the fiber direction. At the completion of each PDA step, the strain is increased by the value of $\Delta\epsilon = 0.0005$. Starting with $\epsilon = 0$, the strain value is increased till the composite fails. For present case, it is decided that the composite fails with the failure of two third of its total $N_\beta \times N_\gamma$ subcells. Note that the Fig. 3.4 shows the common flowchart for the analysis of both SFC fragmenattion analysis (Section 4.3) and the analysis of SFC-RVE (Section 4.2). In the case of SFC-RVE, the procedure of length effect in the damage modeling is omitted.
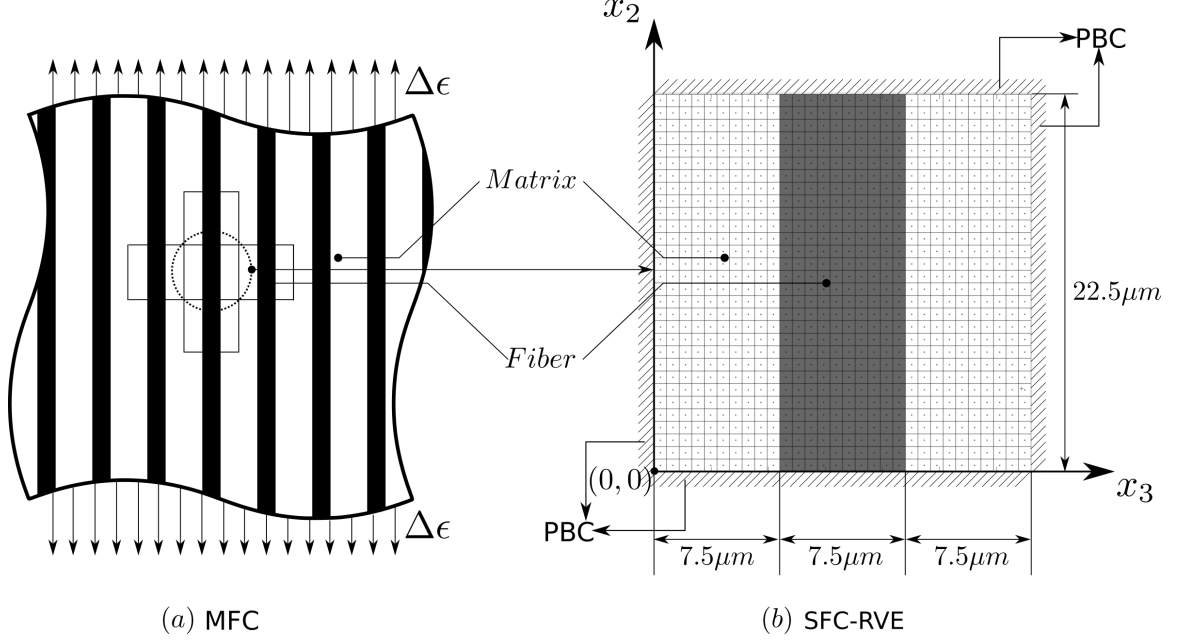
Figure 4.1: Model for SFC-RVE analysis

4.2.4 Assumptions for the analysis of SFC-RVE

Assumptions made for the analysis of SFC-RVE are listed below:

- Fiber are perfectly embedded in the matrix at regular interval.

- Matrix and fiber are assumed to be isotropic.

- It is assumed that there is perfect bonding between matrix and fiber.

- RUC is assumed to be RVE.

- MFC is assumed to be transversely isotropic.

Using aforementioned procedure (Section 4.2), the effective material properties of MFC are evaluated and are presented in the Section 5.1.

4.3 Fiber fragmentation test of Single Fiber Composite

The schematic of the SFC is shown in Fig. 4.2 in which a single fiber filament is embedded in the matrix. In the fiber fragmentation test of SFC, the test piece is loaded with uniaxial tensile load and the loading is applied until each fiber fragment is shorter than the critical length l_c. The concept of critical length l_c has been discussed in the Section 4.3.1. For the PDA analysis of SFC with fiber breakages, strength of the fiber at the smaller length has to be predicted. It is accomplished by the use of Weibull tensile strength distribution [43] of the fiber. It has been discussed in Section 4.3.2. The details of material and geometric parameter for the analysis are discussed in Section 4.3.3. The analysis provides the stress distribution in the SFC with fiber breakages. Distribution of stress at the site of fiber failure gives the direction of matrix crack propagation and the fiber/matrix interface failure. Results of the numerical analysis of the fiber fragmentation test of SFC have been discussed in Section 5.2.
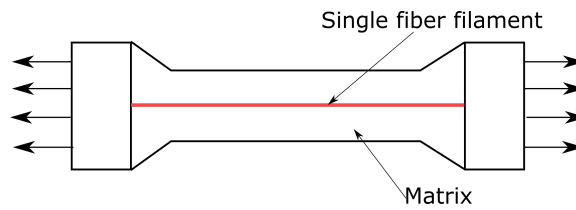

Figure 4.2: Single fiber embedded in a matrix

4.3.1 Critical length for fibers

The load transfer mechanism between the matrix and fiber is explained by using a single fiber composite. Theory of critical length l_c is required in understanding interface stresses between the fiber and matrix. It has been reviewed from the work of Curtin [8, 9, 44]. In order to understand the stress distribution along the fiber-matrix interface, the Kelly & Tyson model [10, 11] has been reviewed briefly in subsequent paragraphs.

To derive the expression for critical length l_c, a small length of fiber in equilibrium is considered. Figure 4.3 shows a small fiber fragment which is in equilibrium under the action of matrix shear τ_m and internal force δF. Eqs. (4.3)–(4.6) have been derived to get an insight of critical length [45].
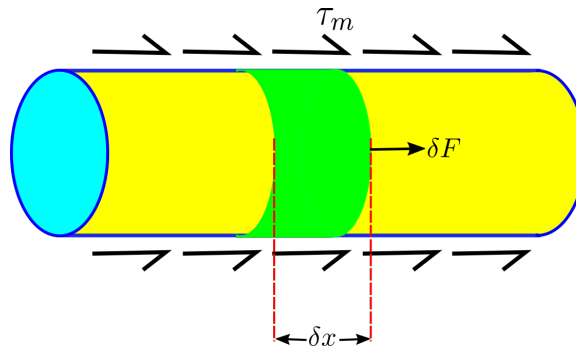

Figure 4.3: Fiber fragment under mechanical equilibrium

31

As shown in the Fig. 4.3, force δF on the small element δx with diameter equal to d is equal to the external matrix shear force. Force equilibrium gives the Eq. (4.3).

$$\delta F = (\pi \tau_m d)\, \delta x \tag{4.3}$$

In order to calculate total force F along the fiber, Eq. (4.3) is integrated from 0 to x.

$$F = \int_0^x (\pi \tau_m d)\, dx \tag{4.4}$$

Assuming a fiber to be of constant cross section area $a = \left(\dfrac{\pi}{4}\right) d^2$, the stress can be obtained from Eq. (4.4) as

$$\sigma(x) = \frac{4}{d} \int_0^x \tau(x) dx \tag{4.5}$$

From Eq. (4.5), it observed that the tensile stress in the fiber increases linearly with increase in x if $\tau(x)$ is constant. For further simplification of the Eq. (4.5), it has been assumed that the shear stress is constant in the small length near the fiber ends [11]. Fig. 4.4 shows the constant shear assumption at the end of fiber. In the zone of the constant shear, tensile stress increases linearly.
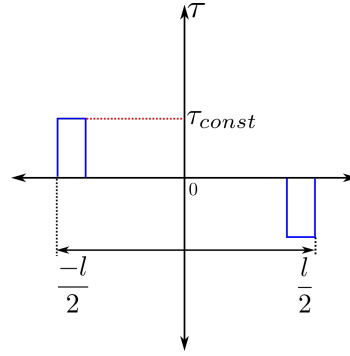

Figure 4.4: Constant shear stress at the fiber ends

The length over which tensile stress increases linearly is termed as a recovery length. After that, the tensile stress remains constant. The constant tensile stress in the fiber mid length is because of the matrix shear on the fiber ends. Thus the maximum stress developed in the fiber is decided by the shear stress on fiber at ends. Consequently, the fiber breaks when the tensile strength developed in the fiber is more than its ultimate tensile strength. Eq. (4.5) is solved for constant matrix shear at the ends of the fiber. Eq. (4.6) is valid only in the zone of constant shear.

$$\sigma(x) = \frac{4\tau_m x}{d} \tag{4.6}$$

Fig. 4.5 assist in realizing the stresses present in the fiber fragments. It is a qualitative illustration of fiber fragmentation test. Readers are encouraged to follow the literature by Netravali et. al [46] in which the detailed study of shear strength at the fiber/matrix interface is conducted experimentally. It shows the tensile stress distribution along the fiber length. Location of zero tensile stress shows

the fiber break points. In Fig. 4.5(a), fiber fragments having the unbroken length can undergo further fracture. In Fig. 4.5(b), fiber fragments still undergoes damage. Further, in Fig. 4.5(c), the length of each fiber fragment is less than the recovery length and hence it cannot take any external loading. It should be observed that there are several fiber fragments of the length l_c, in which the tensile stress is equal to that of the ultimate strength. The term l_c is the critical length of the fiber.
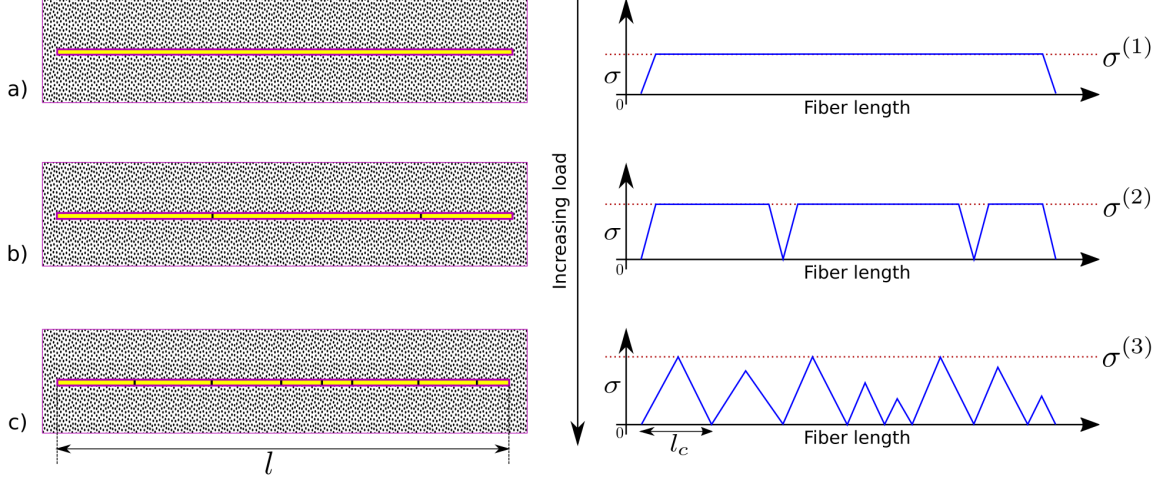

Figure 4.5: Stress distribution in fiber fragments

The critical length l_c is evaluated considering the limiting value of ultimate tensile strength σ_{ult} in the Eq. (4.6).

$$\sigma_{ult} = \frac{2 l_c \tau_m}{d} \tag{4.7}$$

Eq. (4.7) is rearranged to get the critical length l_c as

$$l_c = \frac{\sigma_{ult} d}{2 \tau_m} \tag{4.8}$$

Note that in Fig. 4.5, the maximum tensile stress in the fiber increases after every successive break $(\sigma^{(1)} < \sigma^{(2)} < \sigma^{(3)})$. The reason for increased fiber strength is discussed in subsequent Section 4.3.2.

4.3.2   Weibull tensile strength distribution

Numerical simulation of the single fiber composite fragmentation test requires the information of the ultimate fiber strength at the smaller length of fiber fragments. Experimental data on tensile testing of a single fiber is available at a relatively longer gauge length of the fiber. This data can be linearly extrapolated to obtain fiber strength at smaller gauge length. But it gives the fiber strength at critical length which is fallible as shown by Piggott [47]. Consequently, the fiber strength dependence on the fiber length has been assumed to follow Weibull distribution [43, 40]. The cumulative failure probability $\chi(\sigma, l)$ for the fiber length of l and the stress σ is given by Eq. (4.9) below.

$$\chi(\sigma, l) = 1 - \exp\left\{ -\frac{l}{l_0} \left(\frac{\sigma}{\sigma_0} \right)^m \right\} \tag{4.9}$$

Where σ_0 and m are the Weibull scale and shape parameter for given fiber. For the failure probability of 63.2% [40], the fiber strength can be related to the fiber length by the Eq. (4.10) given below

$$\frac{\sigma}{\sigma_0} = \left(\frac{l_0}{l}\right)^{\frac{1}{m}} \tag{4.10}$$

The maximum strength of broken fiber fragments is found out with the help of Eq. (4.10). Weibull scale σ_0 is termed as the mean strength of the fiber at the gauge length of l_0. The variability in the strength is denoted by Weibull shape parameter m where σ_0 and m are determined experimentally, and they are found to be greater than zero [40]. It implies that for the length $l < l_0$, $\sigma > \sigma_0$. The detailed explanation of the Eq. (4.9) is shown in the Appendix D.

4.3.3 Numerical simulation of SFC fragmentation test with PDA

The numerical analysis of fragmentation of SFC has been discussed in this section. Fig. 4.6 shows the dimensions and the components of the SFC structure that have been used in the PDA. Unidirectional carbon fiber reinforced in the ceramic matrix (FRCMC) has been used for the analysis. The properties of carbon fiber and ceramic matrix (taken from Cheng et al. [27]) are listed in the Table 4.3.

Table 4.3: Properties: Carbon fiber and Ceramics Matrix

	Carbon fiber	Ceramic Matrix
Young's Modulus (GPa)	$E_f = 300$	$E_m = 140$
Poisson's ratio	$\nu_f = 0.2$	$\nu_m = 0.2$
Weibull shape parameter	$m = 3.6$	$--$
Gauge length (mm)	$l_0 = 50$	$--$
Mean tensile strength (MPa) at gauge length	$\sigma_0 = 2500$	$--$
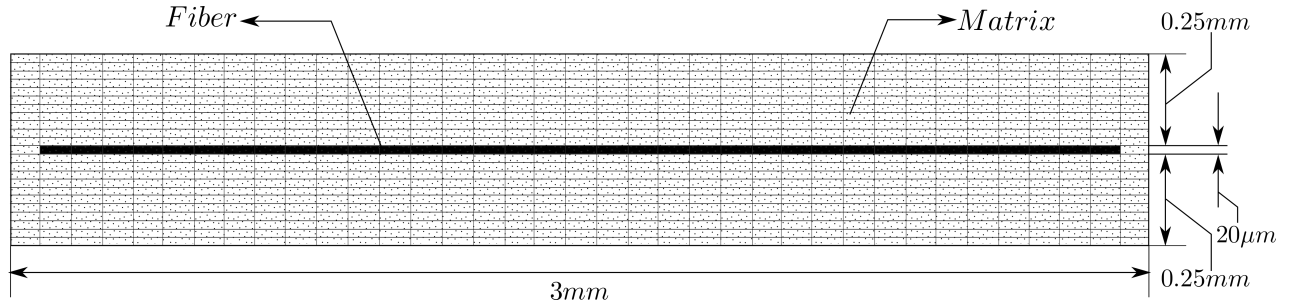
Figure 4.6: Discretized model of SFC for the fiber fragmentation test

In order to conduct the stress analysis with HFGMC methodology, SFC shown in Fig. 4.6 has been discretized into 23×37 number of subcells. These are $N_\beta \times N_\gamma$ respectively. N_β is in the x_2 axis and N_γ is in x_3 axis (see Fig. 2.1 for reference). Such type of discretization allows for the desired micro dimensions of the fiber in Fig. 4.6.

4.3.4 Assumptions in the analysis of SFC fiber fragmentation test

Few assumptions have been made while conducting the numerical analysis of fiber fragmentation in SFC. These are:

- Fiber is assumed to be flawless (homogeneous). This allows the next fiber break to occur at the subcell having highest equivalent tensile stress.

- Ceramic matrix is allowed to take high strains. It helps to carry out the progressive failure of the fiber.

- The strength of the fiber fragment is assumed to be size dependent that is the tensile strength increases with the decrease in length. The strength variation follow the Weibull tensile strength distribution (Section 4.3.2).

- Perfect bonding is considered between the matrix and the fiber. The assumption of perfect bonding has been proved reasonable in the work of McCartney [48] and Parambil & Gururaja [49] as far as the longitudinal loading of a unidirectional composite is considered.
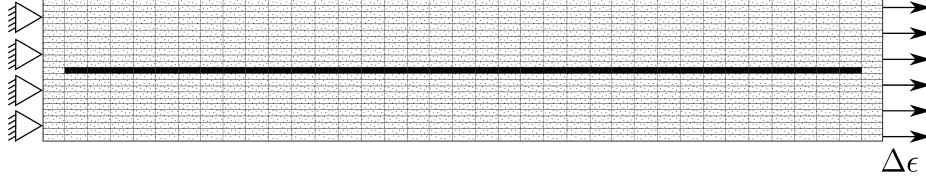

Figure 4.7: Loading diagram for SFC fiber fragmentation test

The SFC shown in the Fig. 4.7 has been loaded longitudinally through the monotonic increase in the strain. Applied strain is incremented by $\Delta\epsilon = 5 \times 10^{-3}$ after every PDA step. To start with, zero strain is applied at the beginning of PDA. HFGMC stress analysis is used in evaluating stress in every subcell. Subsequently, each fiber subcell is checked for damage. The principle stress criteria have been used for the damage detection. Fiber subcell is marked as damaged when the equivalent tensile stress exceeds the strength limit. Fracture index (FI) is quantified for every subcell $\beta\gamma$ which is defined as

$$FI^{\beta\gamma} = \frac{\sigma^{\beta\gamma}}{X^{\beta\gamma}} \tag{4.11}$$

where $X^{\beta\gamma}$ is the maximum tensile strength of the $\beta\gamma$ subcell. If the fracture index $FI^{\beta\gamma} \geq 1$, it implies that the subcell $\beta\gamma$ has failed. The properties of failed subcells are suddenly degraded. For the present analysis, the degradation factor is chosen to be ad hoc and has been kept equal to 99%. It cannot be 100% as it would leave the stiffness matrix singular. Along with this, the degradation factor of 99% ensures that the failed subcells do not transfer any load in the subsequent PDA step. Same procedure is followed for every strain increment till the stopping criteria is met. Simulation is terminated when the fiber reaches its critical length. Results of the single fiber fragmentation test are presented in Section 5.2.

Chapter 5

Results and discussion

Results of the analyses described in the Sections 4.2 and 4.3 have been presented in the current chapter. While Section 5.1 provides results of the analysis of CFRP composites with the representative volume element of single fiber composite (SFC-RVE), Section 5.2 provides the discussion on the results obtained in the SFC fiber fragmentation test. Inferences derived in Section 5.1 are based on the observation of stiffness matrix and homogenized stress-strain curve. Geometrical and material details required in the multi-fiber composite analysis with SFC-RVE are provided in Sections 4.2.1 and 4.2.3.

The outcome of the fiber fragmentation test in SFC are detailed in Section 5.2. It comprises of the discussion on stress re-distribution in SFC as a consequence of fiber fragmentation. Section 4.3.3 contains the information on the material and geometrical parameters required in the SFC fiber fragmentation test. Further, a common progressive damage analysis framework summarized in Fig. 3.4 is used in conducting numerical simulations.

5.1 Effective property calculations of multi fiber composite

Present section provides a detailed discussion on the results obtained by the progressive damage analysis (PDA) of SFC-RVE. Analysis information is available in Section 4.2 where a single RVE is loaded with a strain in the direction of the fiber. Further the applied strain was increased monotonically by $\Delta\epsilon = 0.0005$ at the completion of each PDA step. Starting with $\epsilon = 0$, the strain is applied till the total of two-third of the $N_\beta \times N_\gamma$ subcells fail. Discretization of SFC-RVE in $N_\beta \times N_\gamma = 30 \times 30$ is required for the HFGMC stress analysis. The schematic of the SFC-RVE is provided in Fig. 4.1 in which geometry of the SFC-RVE to be analyzed is square having the sides of 22.5 μm. Fiber diameter is kept 7.5 μm. Such dimensions are required to simulate the experimental testing of multi-fiber CFRP composite conducted by Kashfuddoja & Ramji [41]. They had used Digital Image Correlation (DIC) technique to find the property values of CFRP composite. Further the results obtained from the numerical simulations are compared with the experimental finding available in the same literature. Analytical estimates based on the rule of mixture (Section 4.2.2) are also provided for comparison with SFC-RVE analysis results. Subsequent paragraphs furnishes results with the help of Fig. 5.1 and Table 4.1. All the results provided are based on the effective stress-strain response of composite upon loading.

Fig. 5.1 shows the homogenized stress-strain response obtained from the numerical analysis of SFC-RVE. The plot has been made till the failure in SFC-RVE is detected. In the present case, SFC-RVE fails with the matrix failure which is detected at a strain of $\epsilon = 4 \times 10^{-3}$. The horizontal axis denotes the increment in strain. Corresponding to each strain increment, a homogenized stress value (in MPa) is calculated and plotted against the vertical stress axis. Thus the three trends are obtained for each of the matrix, fiber and composite. From the figure, it is observed that the effective stiffness property of composite lie between the fiber and the matrix.
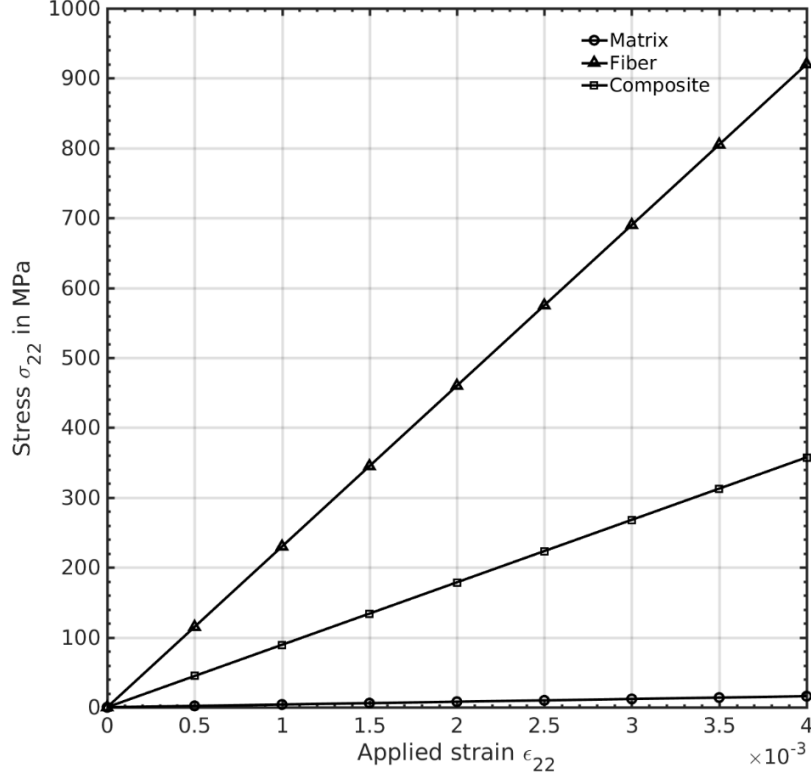

Figure 5.1: Homogenized stress-strain curve for SFC-RVE analysis

The strain at the fiber/matrix interface is equal as it has been assumed in Section 4.2.4 that there is a perfect bond between fiber and matrix. Thus it follows that

$$\epsilon_f = \epsilon_m$$

$$\frac{\sigma_f}{E_f} = \frac{\sigma_m}{E_m}$$

E_f and E_m are obtained with the help of relation $E = 2G(1 + \nu)$ (Table 4.2 gives the value of shear modulus G and Poisson's ratio ν). Using these values in the above equation it is seen that the fiber is 60 times more stressed than the matrix. The matrix does not take part in the loading but its primary function is to transfer the load to the fiber. Hence the matrix reinforcement is required in composite even if there is an overall decrease in its stiffness property as compared to the fiber.

Numerical simulation provides effective properties in the direction of the fiber. It estimates the longitudinal modulus E_{11} to be $89.37\ GPa$. Table 5.1 gives the results based on the analysis of

SFC-RVE, and it has been compared with the experimental and analytical results. Analytical results are based on the rule of mixture. The longitudinal modulus E_{11} calculated on the basis of HFGMC analysis is deviating from the experimental findings with an error of 9.13%. Hence the assumption of one repeating unit cell is equal to the representative volume element, stated in Section 4.2.4, has to be researched. Though there is a deviation between the numerical analysis of SFC-RVE from the experimental findings, the results obtained are used in the qualitative explanation of the load transfer between the fiber and the matrix.

Table 5.1: Comparison between numerical, experimental and analytical results

	Longitudinal modulus, E_{11} GPa	In-plane Poisson's ratio, ν_{12}
Numerical simulation	89.37	0.30
Experimental findings	81.90	0.34
Analytical estimates	81.47	0.34

The stiffness matrix for the multi fiber composite is shown in Eq. (5.1) which is obtained from the SFC-RVE analysis. The stiffness matrix shows the transversely isotropic nature of unidirectional CFRP composite under analysis.

$$\left\{\begin{array}{c} \sigma_{11} \\ \sigma_{22} \\ \sigma_{33} \\ \sigma_{23} \\ \sigma_{31} \\ \sigma_{12} \end{array}\right\} = \left[\begin{array}{cccccc} 89375 & 28431 & 4403 & 0 & 0 & 0 \\ 28431 & 89375 & 4403 & 0 & 0 & 0 \\ 4403 & 4403 & 9054 & 0 & 0 & 0 \\ 0 & 0 & 0 & 2198 & 0 & 0 \\ 0 & 0 & 0 & 0 & 2198 & 0 \\ 0 & 0 & 0 & 0 & 0 & 30472 \end{array}\right] \left\{\begin{array}{c} \epsilon_{11} \\ \epsilon_{22} \\ \epsilon_{33} \\ \epsilon_{23} \\ \epsilon_{31} \\ \epsilon_{12} \end{array}\right\} \qquad (5.1)$$

5.2 SFC analysis for the fiber fragmentation test

Detailed discussions on the results of SFC fiber fragmentation test is presented in subsequent sections. The result of the present work provide the stress contours of progressively damaged SFC. The average tensile and shear stress contours are discussed to understand the stress redistribution and fiber-matrix debonding in the SFC. The anti-plane shear present at the fiber end causes the interface to fail. The plot of average tensile stress along the fiber length gives the indication of increased fiber strength after the fiber fracture. Further, the stress transfer at the fiber ends is also explained. Results under the present analysis are classified into four categories.

- Stress redistribution

- Matrix fiber interface failure

- Average tensile stress distribution in the fiber

- Stress interactions along the fiber-matrix interface

In order to conduct the fiber fragmentation test of SFC, PDA framework briefed in Fig. 3.4 is used. All the results derived in current section are obtained on the common problem definition discussed in Section 4.3.3 where the strain is applied in the direction of the fiber. The external longitudinal load is applied with an increment of $\Delta\epsilon = 0.0005$ at the end of each PDA step. The monotonic load increment is applied till the stopping criteria of achieving the critical length l_c is met (Section 4.3.1). Further, the output obtained in the analysis are post processed in MATLAB. They follow in subsequent sections:

5.2.1 Stress redistribution

Fig. 5.2 shows the average tensile stress contour and the stress redistribution after the fiber breakage. Color-bar accompanying each sub-figure indicates the average tensile stress in megaPascals (MPa). It consists of four figures depicting the progressive failure. Note that the figure shows the maximum stress the fiber can take just before the next breakage. The vertical and the horizontal axis for each of the four figures is showing N_β and N_γ respectively. Each subplot in Fig. 5.2 has been plotted at the maximum value of strain the fiber can take such that the damage is induced in the next PDA step. Plots have been made at a strain value of 1.8%, 2.2%, 2.65% and 2.75%.

The maximum stress taken by the fiber decreases just after the new break. As a result of the stress redistribution, SFC continues to take stress after the damage. It happens as a result of the increased fiber strength. Thus the residual strength of the SFC increases.

The average stress is maximum at the center of the fiber, and it reduces to zero at its end. Similar observations are presented by Wu et al. [50] in which authors had conducted the fiber fragmentation process in SFC with finite element procedure. In the same figure, failure strain is increasing which is attributed to the increased fiber strength. Fiber strength is varying with the number of breaks. It increases with the reduction in fiber length. Thus the increased fiber strength results in increased failure strain.

The redistributed stress also provides the region of maximum stress in the matrix. As it can be observed from the Fig. 5.2(c), the cross X pattern shows the possible direction of matrix cracking. The cross X pattern traces matrix subcells which are having higher strain than the surrounding subcells. It is consistent with the finite element analysis and experimental analysis of fiber fragmentation test presented by Wang et al. [51]. The matrix crack pattern is witnessed around every failed subcell. Zero stresses are present in the failed subcells (as can be seen in Fig. 5.2((b),(c) & (d)) and it is the site at which the matrix and interface failure emanate.

5.2.2 Matrix fiber interface failure

Fig. 5.3 shows the shear stress distribution in the SFC. Most stressed subcells around the fiber break will result in the matrix and interface failure. The region of maximum anti-shear around the fiber breaks has been shown with the lobes drawn around them. Positive shear stress is captured in the continuous lobe. The maximum positive and negative shear around the fiber break causes the interface to fail. Further, it should be noticed that the shear stress in the matrix subcells present along the fiber matrix interface is zero except those that are present at the ends of the fiber. Consequently, the stress transfer between fiber and matrix happens at the ends of fiber fragments. It is further explained in the Section 5.2.4.
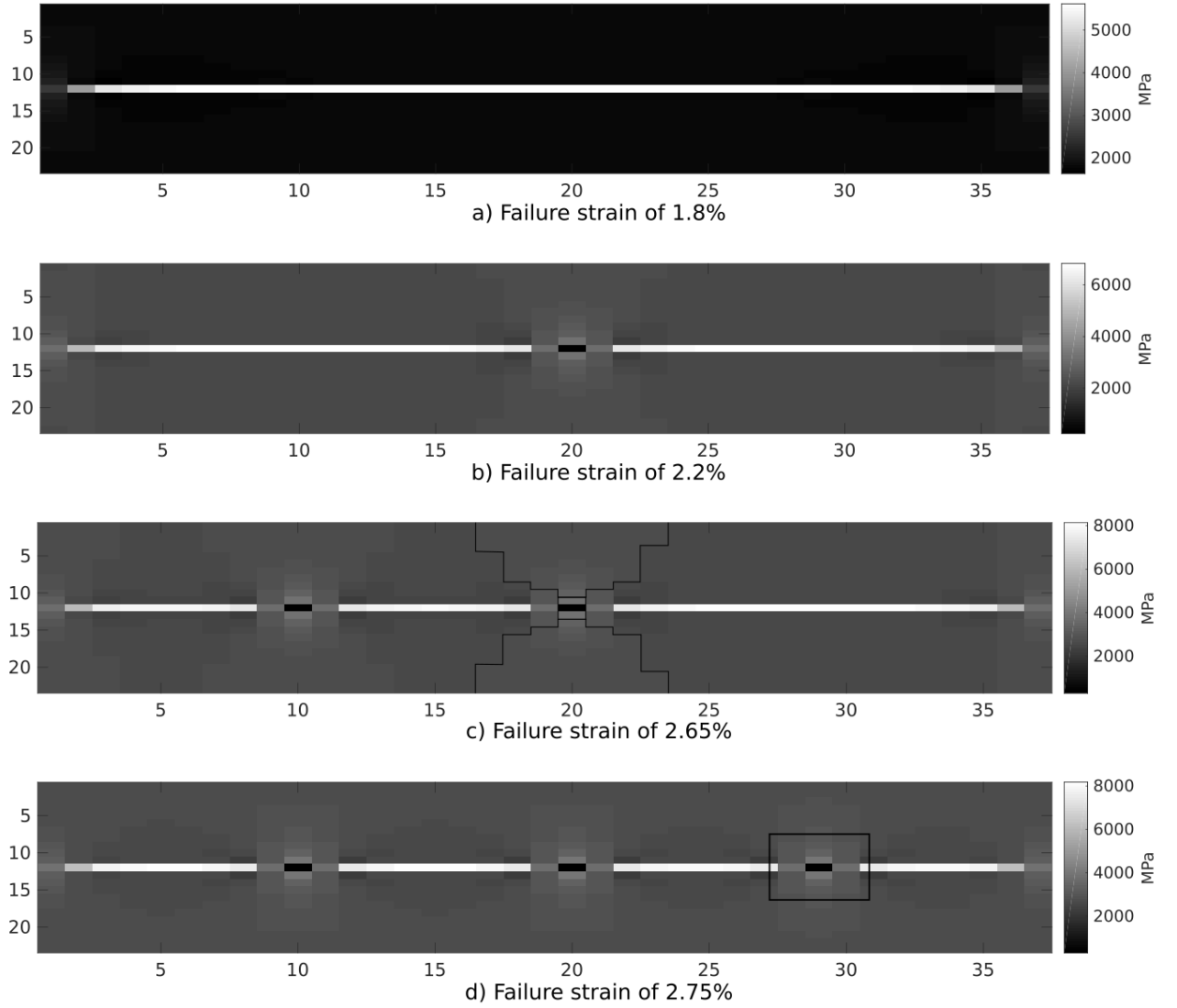
Figure 5.2: Average tensile stress redistribution with progressive damage in the SFC

5.2.3   Average tensile stress distribution in the fiber

Average tensile stress distribution along the fiber length is shown in Fig. 5.4. Fiber stress is plotted against the fiber length of $2.8mm$. There is an increase in the tensile strength as is evident from the Fig. 5.4. It is due to the statistical fiber strength distribution as discussed in the Section 4.3.2.

5.2.4   Stress interactions along the fiber-matrix interface

Fig. 5.6 assists in capturing the stress transfer that occurs at the ends of the fiber. Average tensile stress is plotted against the fiber length in Fig. 5.6(a)while the average shear stress is plotted against the fiber length in Fig. 5.6(b) which consists of two different trends. These trends represent the average shear stress present in the matrix subcells that are immediately neighboring the fiber subcells. Matrix subcells adjacent to the fiber are apprehended in Fig. 5.5. $y \rightarrow \delta^{+}$ and $y \rightarrow \delta^{-}$
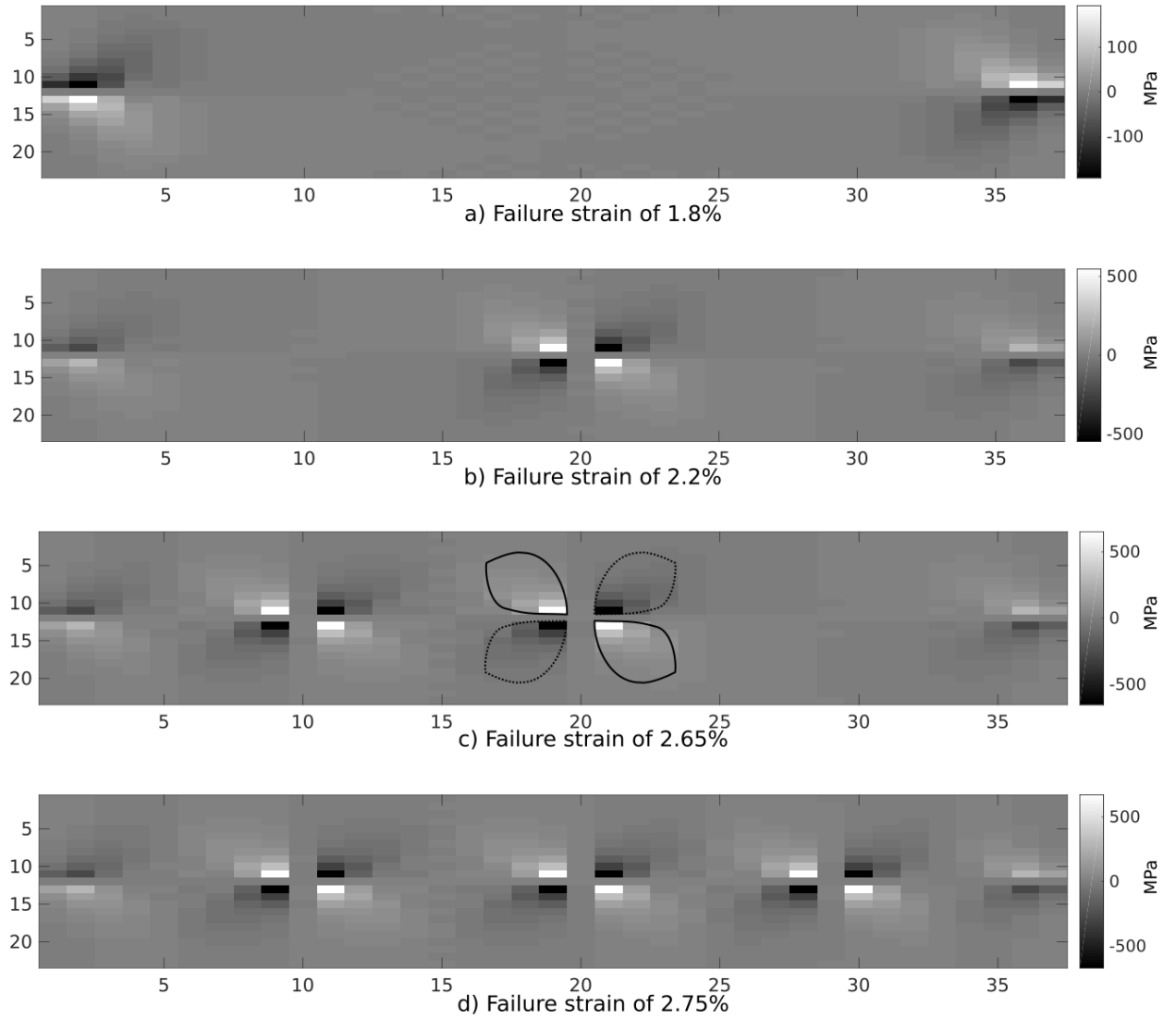
Figure 5.3: Shear stress contour in the SFC

correspond to the bottom and the top interface between the fiber and the matrix. 2δ represents the fiber diameter and $y - axis$ is perpendicular to the fiber axis.

It is realized that the maximum average shear stress is present in the matrix subcells which occupy the neighborhood of fiber ends. Elsewhere it is zero. Section 4.3.1 discussed the theory on tensile stress development in the fiber. It is the zone of stress transfer. Similar trends are obtained in the present analysis such that the tensile stress development happens only in the region of non-zero shear stress. Away from the fiber ends the tensile stress is constant and maximum.
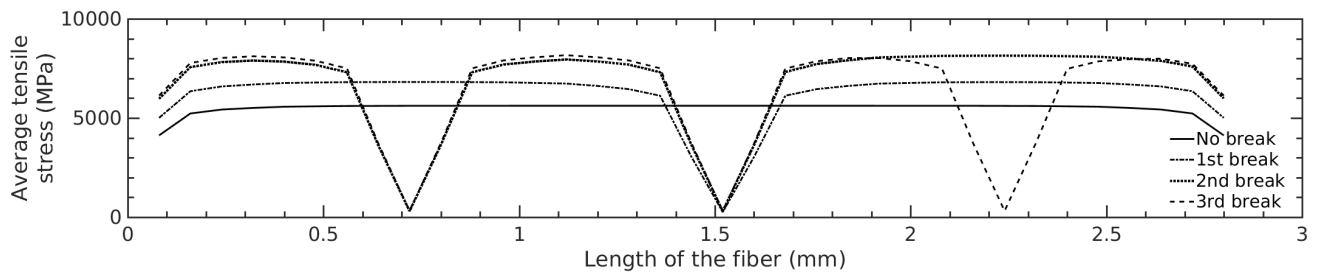
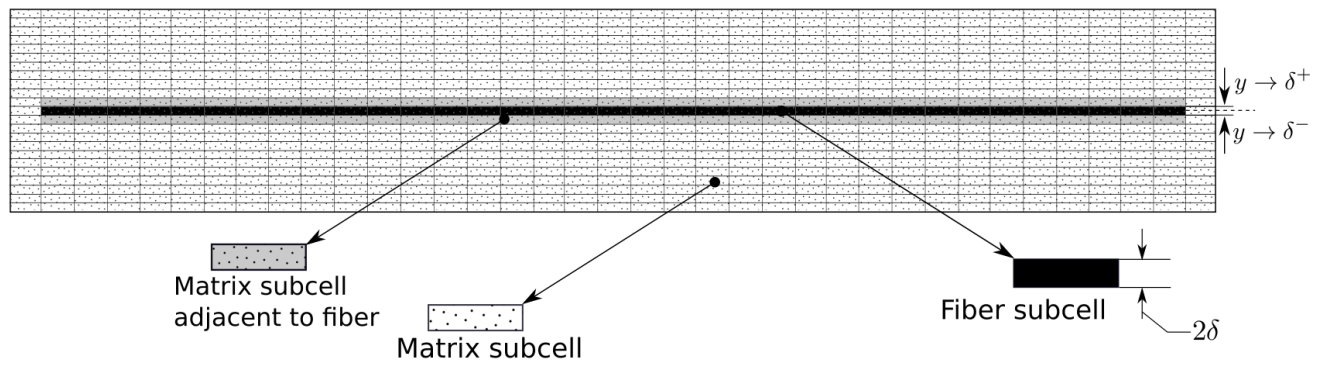Figure 5.4: Average tensile stress along the fiber axis

Figure 5.5: Figure showing the matrix subcells causing stress transfer to the fiber
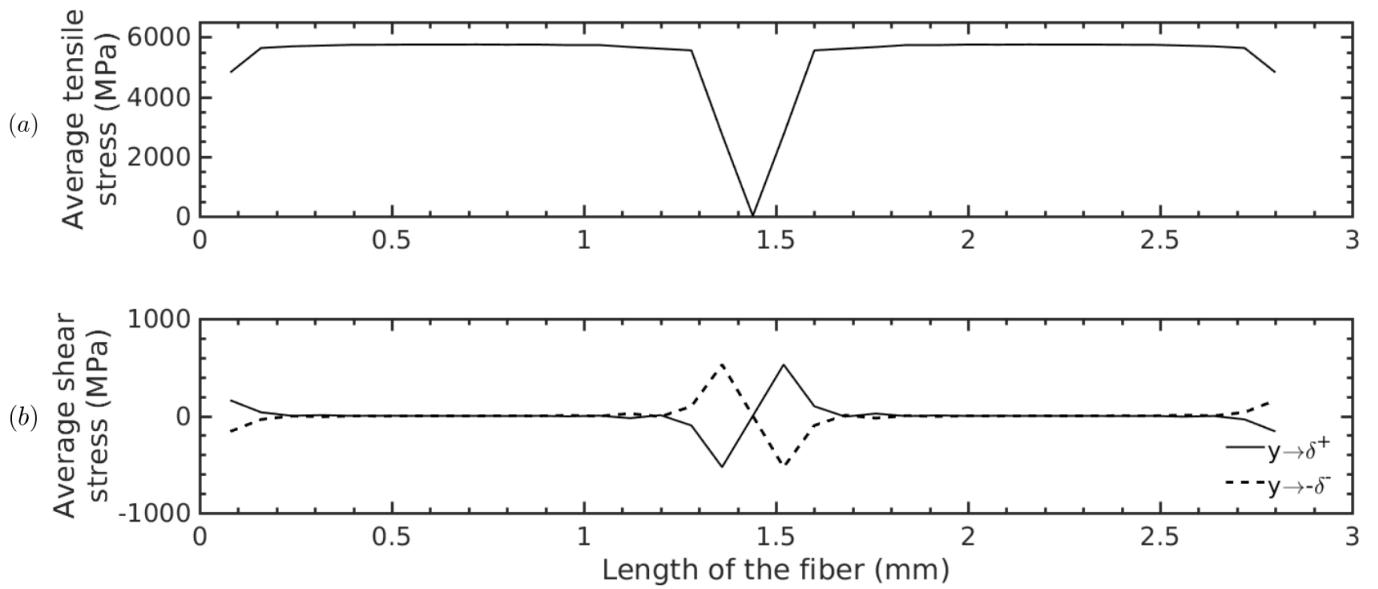

Figure 5.6: Stress transfer mechanism at the ends of fiber; (a) Average tensile stress along the fiber subcells; (b) Average shear stress plot at the fiber matrix interface

Chapter 6

Conclusion and future work

6.1 Conclusion

Single fiber composite (SFC) has been analyzed with progressive damage analysis (PDA). A numerical study has been carried out using the PDA framework that is devised in FORTRAN. Results obtained out of this work have been discussed in Chapter 5. Micro-mechanical studies have been performed for SFC with fiber breakages. It has provided an insight of stress distribution between matrix and fiber. Stiffness properties obtained for multi-fiber composite have been compared with experimental and analytical results.

In Section 5.1, effective property estimation based on the representative volume element has been discussed. Results are used in explaining the effective stiffness of composite. Apart from this, the transverse isotropic nature of unidirectional CFRP composite is also discussed. Importance of matrix reinforcement in composite is understood and realized how matrix assists in transferring load to the fiber.

All of the work done has provided a better intuition of stresses arising in the SFC while it is loaded longitudinally. As discussed in Section 5.2, stress redistribution direction is visualized. As a result of the stress redistribution around the fiber breaks, the composite continues to take the stress. As a result of which successive fragmentation is observed at higher value of strain.

The maximum shear stress region around the fiber ends give the information of fiber-matrix interface failure. Because of the anti-plane shear present at the end of fiber, the interface between fiber and matrix will fail.

Apart from this, the increase in the residual strength of the composite is also discussed. Since the fiber strength increases with decrease in its length, the overall strength of the composite increases and the successive fiber fragmentation happens at increased value of strain.

Toward the end of the Chapter 5, stress interactions along the fiber-matrix interface are presented. It is observed that the load transfer between the fiber and matrix happens at the ends of the fiber. Shear stress applied by matrix at the ends of fiber develops longitudinal tensile stress in the fiber. Also, the zero shear stress in the mid-length of the fiber confirms that the load transfer interactions between fiber and matrix happen only at the end of the fiber.

6.2 Future work

The PDA code developed so far in FORTRAN has the capability to correctly estimate the effective properties of the multiphase structure. The code allows discretization of multiphase structure upto 45×45 (details are provided in Appendix B). Extensive discretization of up to 200×200 is still required to analyze multiphase structures having more than two different phases. It would require the analysis of global stiffness matrix and research for the best possible subroutine available in the literature.

The current PDA analysis allows for the analysis of two-dimensional structures. Three-dimensional HFGMC formulation has to be developed based on the information available in literature [18]. Provision of isoparametric formulation will allow for arbitrary discretization of the structure with quadrilateral shapes other than squares and rectangles. It is known as isoparametric subcell generalization.

Bibliography

[1] E. J. Barbero. Introduction to composite materials design. CRC press, 2010.

[2] A. K. Noor, S. L. Venneri, D. B. Paul, and M. A. Hopkins. Structures technology for future aerospace systems. *Computers & Structures* 74, (2000) 507–519.

[3] J. Aboudi. Micromechanical analysis of composites by the method of cells-update. *Applied Mechanics Reviews* 49, (1996) S83–S91.

[4] Z. Hashin. Analysis of composite materials. *Journal of Applied Mechanics* 50, (1983) 481–505.

[5] S. M. Arnold, B. A. Bednarcyk, A. Hussain, and V. Katiyar. Micromechanics-based structural analysis (FEAMAC) and multiscale visualization within Abaqus/CAE environment .

[6] P. K. Ilankeeran, P. M. Mohite, and S. Kamle. Axial tensile testing of single fibres .

[7] B. A. Budiman, K. Takahashi, K. Inaba, and K. Kishimoto. A new method of evaluating interfacial properties of a fiber/matrix composite. *Journal of Composite Materials* 49, (2015) 465–475.

[8] W. Curtin. Exact theory of fibre fragmentation in a single-filament composite. *Journal of Materials Science* 26, (1991) 5239–5253.

[9] W. A. Curtin. Theory of Mechanical Properties of Ceramic-Matrix Composites. *Journal of the American Ceramic Society* 74, (1991) 2837–2845.

[10] A. Kelly and W. Tyson. Tensile properties of fibre-reinforced metals: Copper/tungsten and copper/molybdenum. *Journal of the Mechanics and Physics of Solids* 13, (1965) 329–338.

[11] S. Zhandarov and E. Pisanova. Two interfacial shear strength calculations based on the single fiber composite test. *Mechanics of composite materials* 31, (1996) 325–336.

[12] J. K. Kim and Y. W. Mai. Engineered interfaces in fiber reinforced composites. Elsevier, 1998.

[13] S. Feih, K. Wonsyld, D. Minzari, P. Westermann, and H. Lilholt. Testing procedure for the single fiber fragmentation test. Technical Report, Forskningscenter Riso 2004.

[14] J. Aboudi. The generalized method of cells and high-fidelity generalized method of cells micromechanical models—A review. *Mechanics of Advanced Materials and Structures* 11, (2004) 329–366.

[15] V. Matonis. The interfacial stresses in particulate composite systems. *Polymer Engineering & Science* 9, (1969) 100–104.

[16] J. Aboudi, S. M. Arnold, and B. A. Bednarcyk. The Generalized Method of Cells Micromechanics. 2013.

[17] R. Haj-Ali and J. Aboudi. Formulation of the high-fidelity generalized method of cells with arbitrary cell geometry for refined micromechanics and damage in composites. *International Journal of Solids and Structures* 47, (2010) 3447–3461.

[18] R. Haj-Ali and J. Aboudi. A new and general formulation of the parametric HFGMC micromechanical method for two and three-dimensional multi-phase composites. *International Journal of Solids and Structures* 50, (2013) 907–919.

[19] J. Aboudi and M. J. Pindera. Micromechanics of metal matrix composites using the generalized method of cells model (gmc) user's guide .

[20] M. H. Sadd. Elasticity: theory, applications, and numerics. Academic Press, 2009.

[21] M. M. Shokrieh and L. B. Lessard. Progressive fatigue damage modeling of composite materials, Part I: Modeling. *Journal of Composite Materials* 34, (2000) 1056–1080.

[22] C. G. Davila, P. P. Camanho, and C. A. Rose. Failure criteria for FRP laminates. *Journal of Composite materials* 39, (2005) 323–345.

[23] M. J. Hinton, A. S. Kaddour, and P. D. Soden. Failure criteria in fibre reinforced polymer composites: the world-wide failure exercise. Elsevier, 2004.

[24] J. S. Mayes. Micromechanics based failure analysis of composite structural laminates. Technical Report, DTIC Document 1999.

[25] P. Nali and E. Carrera. A numerical assessment on two-dimensional failure criteria for composite layered structures. *Composites Part B: Engineering* 43, (2012) 280–289.

[26] D. Mendels. Analysis of the single-fibre fragmentation test. NPL, 2001.

[27] T. Cheng, R. Qiao, and Y. Xia. A Monte Carlo simulation of damage and failure process with crack saturation for unidirectional fiber reinforced ceramic composites. *Composites science and technology* 64, (2004) 2251–2260.

[28] W. Drugan. Two exact micromechanics-based nonlocal constitutive equations for random linear elastic composite materials. *Journal of the Mechanics and Physics of Solids* 51, (2003) 1745–1772.

[29] T. Kanit, S. Forest, I. Galliet, V. Mounoury, and D. Jeulin. Determination of the size of the representative volume element for random composites: statistical and numerical approach. *International Journal of Solids and Structures* 40, (2003) 3647–3679.

[30] Z. Hashin. Failure criteria for unidirectional fiber composites. *Journal of applied mechanics* 47, (1980) 329–334.

[31] P. Papanikos, K. Tserpes, and S. Pantelakis. Modelling of fatigue damage progression and life of CFRP laminates. *Fatigue & Fracture of Engineering Materials & Structures* 26, (2003) 37–47.

[32] Y. S. Reddy and J. N. Reddy. Three-dimensional finite element progressive failure analysis of composite laminates under axial extension. *Journal of Composites, Technology and Research* 15, (1993) 73–87.

[33] M. R. Garnich and V. M. Akula. Review of degradation models for progressive failure analysis of fiber reinforced polymer composites. *Applied Mechanics Reviews* 62, (2009) 010,801.

[34] Intel Math Kernel Library. Reference Manual. Santa Clara, USA. ISBN 630813-054US.

[35] C. G. Petra, O. Schenk, M. Lubin, and K. Gärtner. An augmented incomplete factorization approach for computing the Schur complement in stochastic optimization. *SIAM Journal on Scientific Computing* 36, (2014) C139–C162.

[36] C. G. Petra, O. Schenk, and M. Anitescu. Real-time stochastic optimization of complex energy systems on high-performance computers. *IEEE Computing in Science & Engineering* 16, (2014) 32–42.

[37] H. Kotakemori, H. Hasegawa, and A. Nishida. Performance evaluation of a parallel iterative method library using openmp. In High-Performance Computing in Asia-Pacific Region, 2005. Proceedings. Eighth International Conference. IEEE, 2005 432–436.

[38] E. Anderson, Z. Bai, C. Bischof, S. Blackford, J. Demmel, J. Dongarra, J. Du Croz, A. Greenbaum, S. Hammarling, A. McKenney, and D. Sorensen. LAPACK Users' Guide. 3rd edition. Society for Industrial and Applied Mathematics, Philadelphia, PA, 1999.

[39] M. Nishikawa, T. Okabe, and N. Takeda. Mechanics of fiber fragmentation in single-fiber composite. In 16th International Conference on Composite Materials. 2007 .

[40] F. M. Zhao, T. Okabe, and N. Takeda. The estimation of statistical fiber strength by fragmentation tests of single-fiber composites. *Composites Science and Technology* 60, (2000) 1965–1974.

[41] M. Kashfuddoja and M. Ramji. An experimental and numerical investigation of progressive damage analysis in bonded patch repaired CFRP laminates. *Journal of Composite Materials* 49, (2015) 439–456.

[42] R. M. Jones. Mechanics of composite materials. CRC press, 1998.

[43] S. Lee, T. Nguyen, J. Chin, and T. Chuang. Analysis of the single-fiber fragmentation test. *Journal of materials science* 33, (1998) 5221–5228.

[44] M. Ibnabdeljalil and W. Curtin. Strength and reliability of fiber-reinforced composites: localized load-sharing and associated size effects. *International Journal of Solids and Structures* 34, (1997) 2649–2668.

[45] X. Jiang and Q. Gao. Stress-transfer analysis for fibre/matrix interfaces in short-fibre-reinforced composites. *Composites science and technology* 61, (2001) 1359–1366.

[46] A. Netravali, R. Henstenburg, S. Phoenix, and P. Schwartz. Interfacial shear strength studies using the single-filament-composite test. I: Experiments on graphite fibers in epoxy. *Polymer Composites* 10, (1989) 226–241.

[47] M. Piggott. Why interface testing by single-fibre methods can be misleading. *Composites Science and Technology* 57, (1997) 965–974.

[48] L. McCartney. New theoretical model of stress transfer between fibre and matrix in a uniaxially fibre-reinforced composite. In Proceedings of the Royal Society of London A: Mathematical, Physical and Engineering Sciences, volume 425. The Royal Society, 1989 215–244.

[49] N. K. Parambil and S. Gururaja. Micro-scale progressive damage development in polymer composites under longitudinal loading. *Mechanics of Materials* 111, (2017) 21–34.

[50] X. Wang, J. Zhang, Z. Wang, W. Liang, and L. Zhou. Finite element simulation of the failure process of single fiber composites considering interface properties. *Composites Part B: Engineering* 45, (2013) 573–580.

[51] X. Wang, B. Zhang, S. Du, Y. Wu, and X. Sun. Numerical simulation of the fiber fragmentation process in single-fiber composites. *Materials & Design (1980-2015)* 31, (2010) 2464–2470.

[52] M. Abramowitz, I. A. Stegun et al. Handbook of mathematical functions. *Applied mathematics series* 55, (1966) 39.

[53] M. A. Cavalcante, E. N. Lages, S. P. Marques, and M.-J. Pindera. The High-Fidelity Generalized Method of Cells with arbitrary cell geometry and its relationship to the Parametric Finite-Volume Micromechanics. *International Journal of Solids and Structures* 49, (2012) 2037–2050.

[54] A. Heckert and J. J. Filliben. Statistical Engineering Division, Information Technology Laboratory. Available at http://www.itl.nist.gov/div898/handbook/eda/section3/eda3668.htm, Accessed on 2017-05-30.

Appendices

Appendix A

HFGMC displacement equation

A.1 Complete and incomplete quadratic equation of displacement in HFGMC method

The general equation for displacement of a subcell in the parametric coordinate is given by:

$$u^{(\beta\gamma)} = \bar{\epsilon}.X + \sum_{m=0}^{M} \sum_{n=0}^{N} \mathbf{w}_{(mn)} P_m(r) P_n(s) \tag{A.1}$$

Expanding the above equation upto second order in r and s, following equation is obtained:

$$\begin{aligned} u^{(\beta\gamma)} = \bar{\epsilon}.X \\ + \mathbf{w}_{(00)} P_0(r) P_0(s) + \mathbf{w}_{(01)} P_0(r) P_1(s) + \mathbf{w}_{(10)} P_1(r) P_0(s) \\ + \mathbf{w}_{(11)} P_1(r) P_1(s) + \mathbf{w}_{(02)} P_0(r) P_2(s) + \mathbf{w}_{(20)} P_2(r) P_0(s) \end{aligned} \tag{A.2}$$

Legendre polynomials [52] $P_0(x)$, $P_1(x)$ and $P_2(x)$ are defined as

$$\begin{aligned} P_0(x) &= 1 \\ P_1(x) &= x \\ P_2(x) &= \frac{1}{2}(3x^2 - 1) \end{aligned} \tag{A.3}$$

Putting the value of $P_0(x)$, $P_1(x)$ and $P_2(x)$ back in the equation Eq. (A.2), following equation is obtained:

$$u^{\beta\gamma} = \bar{\epsilon}.X + \mathbf{w}_{(00)} + r\mathbf{w}_{(10)} + s\mathbf{w}_{(01)} + rs\mathbf{w}_{(11)} + \frac{1}{2}\mathbf{w}_{(20)}\left(3r^2 - 1\right) + \frac{1}{2}\mathbf{w}_{(02)}\left(3s^2 - 1\right) \tag{A.4}$$

Above is the complete form of HFGMC displacement equation in parametric form. When the subcell array arrangement is orthogonal, the term $\mathbf{w}_{11}$ is zero. The incomplete HFGMC formulation in the

local coordinate system (y_2^β, y_3^γ) is:

$$u^{\beta\gamma} = \bar{\epsilon}.X + \mathbf{w}_{(00)}^{\beta\gamma} + y_2^{(\beta)}\mathbf{w}_{(10)}^{\beta\gamma} + y_3^{(\gamma)}\mathbf{w}_{(01)}^{\beta\gamma} + \frac{1}{2}\left(3y_2^{(\beta)2} - \frac{h_\beta^2}{4}\right)\mathbf{w}_{(20)}^{\beta\gamma} + \frac{1}{2}\left(3y_3^{(\gamma)2} - \frac{l_\gamma^2}{4}\right)\mathbf{w}_{(02)}^{\beta\gamma}$$

(A.5)

In the case of parametric HFGMC analysis [53], the term $rs\mathbf{w}_{11}$ is retained in the displacement equation. It is due to the non orthogonality in subcell arrangement such that the *dot* product of the rs in Eq. (A.4) does not vanish.

Appendix B

System of linear equation in HFGMC analysis

B.1 Least square solution of the problem $A \times x = b$

The least square solution helps in determining the solution of overdetermined system (where number of constraints are more than the unknowns) and the solution of the problem where the unique common solution does not exist. In such a case, least square solution is predicted which gives the least error as compared to other possible solutions. Derivation of the linear least squares is given below:

Let the most correct solution of the system of the equation $A \times x = b$ is b and let it gives the error of e. Thus the expression for error e is:

$$Ax - b = e \tag{B.1}$$

The sum squared error ($SSE = e^T e$) is given as:

$$SSE = (Ax - b)^T (Ax - b) \tag{B.2}$$

As the transpose operator is distributive over the product, we have $(Ax - b)^T = (x^T A^T - b^T)$. Hence,

$$SSE = (x^T A^T - b^T)(Ax - b) \tag{B.3}$$

With matrix pre-multiplying operation, we have,

$$SSE = x^T A^T Ax - x^T A^T b - b^T Ax + b^T b \tag{B.4}$$

The middle two terms of Eq. (B.4) are transpose of each other and can be added. Thus

$$SSE = x^T A^T Ax - 2x^T A^T b + b^T b \tag{B.5}$$

Since the SSE has to be minimum, its partial derivative with respect to x is evaluated and then equated to zero to get the least error solution.

$$\begin{aligned}
\frac{\partial SSE}{\partial x} &= \frac{\partial}{\partial x}(x^T A^T A x - 2x^T A^T b + b^T b) \qquad &\text{(B.6)} \\
&= A^T A x + x^T A^T A - 2A^T b \\
&= 2A^T A x - 2A^T b
\end{aligned}$$

Equating the SSE to 0, we have

$$A^T A x = A^T b \qquad \text{(B.7)}$$

Multiplying both the sides by $(A^T A)^{-1}$, we have

$$x = (A^T A)^{-1} A^T b \qquad \text{(B.8)}$$

This solution of the Eq. (B.8) given the least error solution, to the system of linear equation. In the HFGMC analysis, the solution of the equation $\Delta X = T_G^{-1} D_G$, is found with the help of Intel Math Kernel Library. '$DGELSD$' is the subroutine used to solve this equation. Other solvers are also used based on the sparsity of the T_G matrix.

B.2   Use of the sparse solvers

Sparse analysis of the T_G matrix is shown in the Table B.1 given below. The number of the subcells are increased on the multiple of three. The analysis shows that the non-zero values comprise less

Table B.1: Analysis of sparsity of T_G matrix

Number of subcells $(N_\beta \times N_\gamma)$	Total non-zero values in T_G matrix	Total number of values in T_G matrix	% of non-zero values
3×3	666	135×135	3.65
6×6	2664	540×540	0.91
9×9	5994	1215×1215	0.406
12×12	10656	2160×2160	0.228
15×15	16650	3375×3375	0.146
18×18	23976	4860×4860	0.1015
21×21	32634	6615×6615	0.0745

of the total T_G matrix. This sparsity helps in utilizing sparse solver libraries like MUMPS, LIS, SuperLU, PARDISO, etc. Further, the structure of the T_G matrix is shown below. Most of the non-zero elements lie on the diagonal of the matrix. Also, the Fig. B.1 shows the extra memory occupied by the zero elements of T_G matrix. White pixels shows the non-zero values. The present PDA code definition in the Section 3.4, PARDISO and LIS sparse solvers have been included.
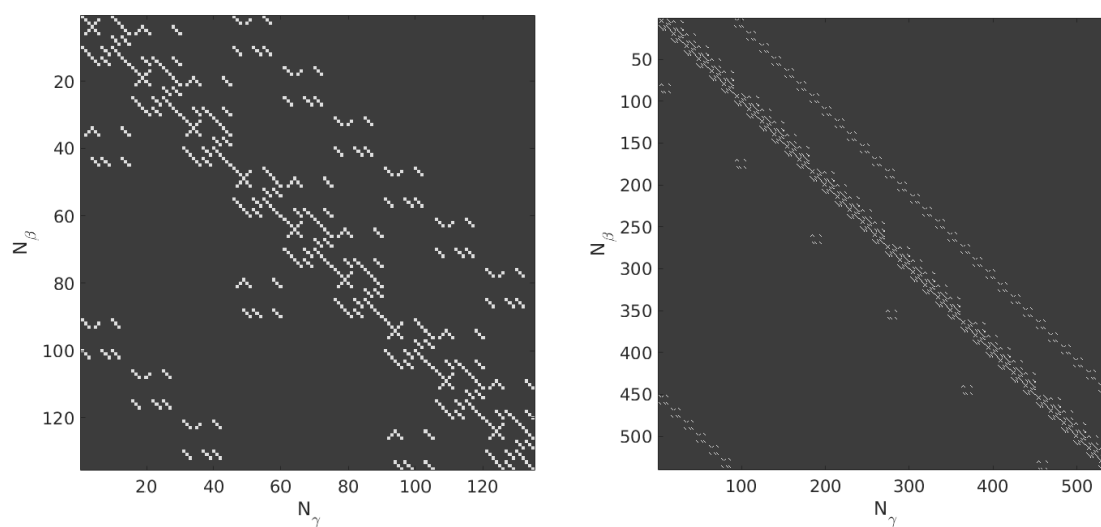
(a) Morphology of 3×3 subcells

(b) Morphology of 6×6 subcells

Figure B.1: Distribution of zeros and non-zeros in T_G matrix

54

Appendix C

Stress and strain expression for multi continuum theory

In the Section 3.2.2, Eq. (3.6) and Eq. (3.7) are derived. These are:

$$\sigma = \sigma_f \phi_f + \sigma_m \phi_m \tag{C.1}$$

$$\epsilon = \epsilon_f \phi_f + \epsilon_m \phi_m \tag{C.2}$$

When the Hooke's law is applied for each of the fiber, matrix and composite separately, following expressions are obtained:

$$\{\sigma_f\} = [C_f]\{\epsilon_f\} \tag{C.3}$$

$$\{\sigma_m\} = [C_m]\{\epsilon_m\} \tag{C.4}$$

$$\{\sigma\} = [C]\{\epsilon\} \tag{C.5}$$

Putting the value of Eqs. (C.4) and (C.5) in Eq. (C.1), following equation is obtained:

$$[C]\{(\phi_f \epsilon_f + \phi_m \epsilon_m)\} = \phi_f [C_f]\{\epsilon_f\} + \phi_m [C_m]\{\epsilon_m\} \tag{C.6}$$

$$[C]\{\phi_f \epsilon_f\} + [C]\{\phi_m \epsilon_m\} = \phi_f [C_f]\{\epsilon_f\} + \phi_m [C_m]\{\epsilon_m\} \tag{C.7}$$

To solve for ϵ_f, Eq. (C.7) is rearranged such that terms in fiber and matrix are separated.

$$[C]\{\phi_f \epsilon_f\} - \phi_f [C_f]\{\epsilon_f\} = \phi_m [C_m]\{\epsilon_m\} - [C]\{\phi_m \epsilon_m\} \tag{C.8}$$

Taking out the terms in common on RHS and LHS, following equation is obtained:

$$\phi_f \left[[C] - [C_f]\right] \{\epsilon_f\} = \phi_m \left[[C_m] - [C]\right] \{\epsilon_m\} \tag{C.9}$$

Thus the value of ϵ_f is obtained as:

$$\epsilon_f = -\frac{\phi_f}{\phi_m} \left([C] - [C_f]\right)^{-1} \left([C] - [C_m]\right) \{\epsilon_m\} \tag{C.10}$$

The term in the multiplication of ϵ_m on the RHS of Eq. (C.10) is taken as $[A]$. Then the above equation becomes:

$$\epsilon_f = [A]\{\epsilon_m\} \tag{C.11}$$

Using the value of $[A]$ in the Eq. (C.2), the value of ϵ_m is obtained as:

$$\{\epsilon\} = [A]\{\epsilon_m\}\phi_f + \{\epsilon_m\}\phi_m \tag{C.12}$$

$$\{\epsilon_m\} = \left(\phi_m[I] + \phi_f[A]\right)^{-1}\{\epsilon\} \tag{C.13}$$

Appendix D

Statistical Weibull distribution

D.1   Fiber strength distribution with Weibull distribution

The standard probability density function (pdf) for the Weibull distribution is given below in Eq. (D.1). It is used in calculating the cumulative distribution function (CDF) used for the determination of the fiber strength. The following derivation has been done based on the literature available at Exploratory Data Analysis [54].

$$f(x) = \frac{m}{\alpha} \left(\frac{x - \mu}{\alpha} \right)^{(m-1)} exp(-((x - \mu)/\alpha)^m) \qquad x \geq \mu; m, \alpha > 0 \tag{D.1}$$

In the above equation, m is the shape parameter, μ is the location parameter and α is the scale parameter. A two-parameter Weibull distribution is obtained by putting $\mu = 0$ and $\alpha = 1$. The two parameter standard Weibull distribution is obtained as in Eq. (D.2).

$$f(x) = mx^{(m-1)}e^{(-x^m)} \tag{D.2}$$

e in the above equation represent exponential exp. To get the cumulative distribution function F, the expression in Eq. (D.2) is integrated in the limit 0 to x.

$$F = \int_0^x mx^{(m-1)}e^{(-x^m)}dx \tag{D.3}$$

Eq. (D.3) can be easily integrated by assuming $u = -x^m$, such that

$$
\begin{aligned}
u &= x^m \\
\frac{du}{dx} &= -mx^{m-1} \\
F &= -\int e^u du \\
F &= -e^u + C
\end{aligned}
\tag{D.4}
$$

Putting back the value of u and solving the Eq. D.5 for the limits, following equation is obtained.

$$F = 1 - e^{-x^m} \tag{D.5}$$

For the statistical distribution of fiber strength, the variable x^m in the Eq. (D.5) is replaced by the term $\frac{l}{l_0} \left(\frac{\sigma}{\sigma_0} \right)^m$. The expression obtained is

$$F = 1 - exp \left(-\frac{l}{l_0} \left(\frac{\sigma}{\sigma_0} \right)^m \right) \tag{D.6}$$

For the cumulative failure probability of 63.2%, the term inside the exponential of Eq. (D.6) should be -1. Thus the following equation is obtained.

$$\sigma = \sigma_0 \left(\frac{l_0}{l} \right)^{\frac{1}{k}} \tag{D.7}$$

Note that at the probability of 63.2%, the Weibull fitted curve intersects the experimental data - least square fitted line [54]. Fig. D.1 shows that the failure probability of 0.632 intersects the Weibull
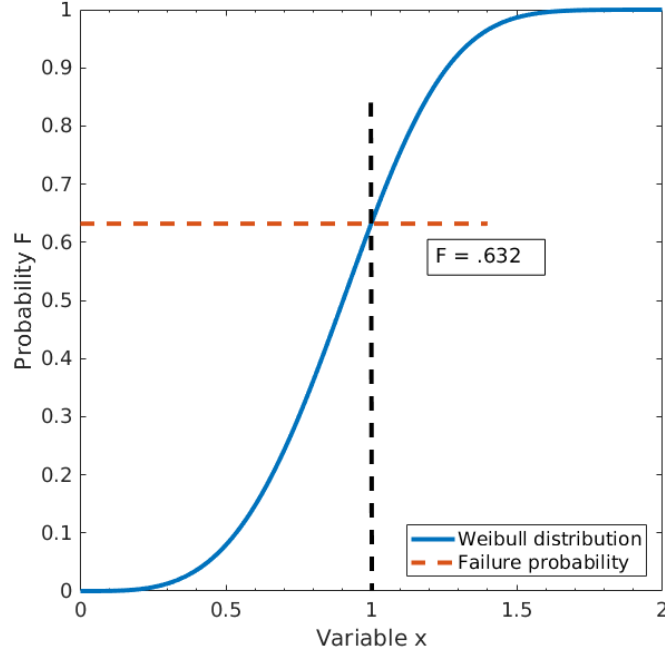

Figure D.1: Weibull plot of the value of m $= 3.6$

curve at $x = 1$. It is the point of intersection of Weibull curve with the experimental data. Note that the above curve is plotted at the shape parameter of $m = 3.6$, which has also been used in the SFC analysis in Chapter 3. Also, the plot shown above is similar to general the Weibull trend for the fiber strength, as can be seen in the literature [40].